Monthly Notices
of the
ROYAL ASTRONOMICAL SOCIETY

MNRAS **444,** 3501–3516 (2014) doi:10.1093/mnras/stu1702

The clustering of galaxies in the SDSS-III Baryon Oscillation Spectroscopic Survey: signs of neutrino mass in current cosmological data sets

Florian Beutler,[1⋆] Shun Saito,[2] Joel R. Brownstein,[3] Chia-Hsun Chuang,[4] Antonio J. Cuesta,[5] Will J. Percival,[6] Ashley J. Ross,[6] Nicholas P. Ross,[7] Donald P. Schneider,[8,9] Lado Samushia,[6] Ariel G. Sánchez,[10] Hee-Jong Seo,[11] Jeremy L. Tinker,[12] Christian Wagner[13] and Benjamin A. Weaver[12]

Affiliations are listed at the end of the paper

Accepted 2014 August 19. Received 2014 August 18; in original form 2014 March 17

ABSTRACT

We investigate the cosmological implications of the latest growth of structure measurement from the Baryon Oscillation Spectroscopic Survey (BOSS) CMASS Data Release 11 with particular focus on the sum of the neutrino masses, $\sum m_\nu$. We examine the robustness of the cosmological constraints from the baryon acoustic oscillation (BAO) scale, the Alcock–Paczynski effect and redshift-space distortions (D_V/r_s, F_{AP}, $f\sigma_8$) of Beutler et al., when introducing a neutrino mass in the power spectrum template. We then discuss how the neutrino mass relaxes discrepancies between the cosmic microwave background (CMB) and other low-redshift measurements within Λ cold dark matter. Combining our cosmological constraints with 9-year *Wilkinson Microwave Anisotropy Probe* (WMAP9) yields $\sum m_\nu = 0.36 \pm 0.14$ eV (68 per cent c.l.), which represents a 2.6σ preference for non-zero neutrino mass. The significance can be increased to 3.3σ when including weak lensing results and other BAO constraints, yielding $\sum m_\nu = 0.35 \pm 0.10$ eV (68 per cent c.l.). However, combining CMASS with *Planck* data reduces the preference for neutrino mass to $\sim 2\sigma$. When removing the CMB lensing effect in the *Planck* temperature power spectrum (by marginalizing over A_L), we see shifts of $\sim 1\sigma$ in σ_8 and Ω_m, which have a significant effect on the neutrino mass constraints. In the case of CMASS plus *Planck* without the A_L lensing signal, we find a preference for a neutrino mass of $\sum m_\nu = 0.34 \pm 0.14$ eV (68 per cent c.l.), in excellent agreement with the *WMAP*9+CMASS value. The constraint can be tightened to 3.4σ yielding $\sum m_\nu = 0.36 \pm 0.10$ eV (68 per cent c.l.) when weak lensing data and other BAO constraints are included.

Key words: surveys – cosmological parameters – cosmology: observations – large-scale structure of Universe.

1 INTRODUCTION

The measurement of neutrino oscillations in neutrino detection experiments using solar, atmospheric and reactor neutrinos has now convincingly shown that neutrinos cannot be massless. Neutrino oscillation experiments are sensitive to the mass differences between the neutrino eigenstates, and the current data imply $|\Delta m^2_{31}| \cong 2.4 \times 10^{-3}$ eV^2 and $\Delta m^2_{21} \cong 7.6 \times 10^{-5}$ eV^2 (Beringer et al. 2012). These measurements provide a lower limit for the sum of the neutrino masses of $\sim$0.06 eV. Using the mass difference constraints above and knowing that $\Delta m^2_{21} > 0$, one can construct two mass hierarchies for neutrinos. The so-called 'normal' hierarchy suggests $m_{\nu_1} < m_{\nu_2} \ll m_{\nu_3}$, where we have one heavy neutrino and two lighter ones, while the so-called 'inverted' hierarchy suggests $m_{\nu_3} \ll m_{\nu_1} < m_{\nu_2}$, where we have one light neutrino and two heavy ones.

Because of the extremely low cross-section of neutrinos it is difficult for laboratory experiments to measure the neutrino mass directly. The current best upper bounds on the neutrino mass from particle physics experiments are from Troitsk (Lobashev et al. 1999) and Mainz (Weinheimer et al. 1999) tritium β-decay experiments that found $m_\beta < 2.3$ eV (95 per cent confidence level), where m_β is the mass to which β-decay experiments are sensitive (see Section 6.2 and equation 21). The Karlsruhe Tritium Neutrino experiment (KATRIN) aims to measure m_β with a sensitivity of $\sim$0.2 eV (Wolf 2010), which would constrain $\sum m_\nu \lesssim 0.6$ eV. Furthermore, neutrinoless double β-decay ($0\nu\beta\beta$) experiments such as

⋆ E-mail: fbeutler@lbl.gov

KamLAND-Zen will assess the effective mass of Majorana neutrinos at the level of $\mathcal{O}(0.1–1)$ eV (Gando et al. 2013) depending on the nuclear matrix element.

With the advent of precision cosmology, it was realized that the neutrino mass has an effect on the matter distribution in the Universe and that this could be used to indirectly measure the sum of the neutrino masses, $\sum m_\nu$. The neutrino mass introduces a scale-dependent suppression of the clustering amplitude with the scale-dependency set by $f_\nu = \Omega_\nu/\Omega_\mathrm{m}$. The suppression of clustering is caused by the large thermal velocity of neutrinos which leads to a large free-streaming scale. Many recent publications have attempted to constrain $\sum m_\nu$, but most were only able to set upper limits (Seljak, Slosar & McDonald 2006; Dunkley et al. 2009; Gong et al. 2008; Hinshaw et al. 2009, 2013; Ichiki, Takada & Takahashi 2009; Li et al. 2009; Tereno et al. 2009; Reid et al. 2010; Thomas, Abdalla & Lahav 2010; Komatsu et al. 2011; Saito, Takada & Taruya 2011; de Putter et al. 2012; Sánchez et al. 2012; Xia et al. 2012; Giusarma et al. 2013; Riemer-Sorensen, Parkinson & Davis 2014; Zhao et al. 2013) with some exceptions based on cluster abundance results (e.g. Hou et al. 2014; Planck Collaboration XX 2013e; Battye & Moss 2014; Burenin 2013; Rozo et al. 2013; Wyman et al. 2014,).

Introducing a neutrino mass suppresses clustering power between the epoch of decoupling and today below the free streaming scale, as massive neutrinos affect the cosmological expansion rate, but free-stream out of matter perturbations. The clustering amplitude is often parametrized by the rms mass fluctuations in spheres of 8 Mpc h^{-1} at the present epoch and denoted σ_8. Given the clustering amplitude at decoupling measured by the cosmic microwave background (CMB), we can predict the $z = 0$ value of σ_8, within a certain cosmological model. However, this σ_8 prediction depends on the initial assumption of the neutrino mass, introducing a degeneracy between σ_8 and $\sum m_\nu$. In fact, if there were no other effect of the neutrino mass on the CMB, the neutrino mass parameter would be completely degenerate with σ_8. Luckily there are several other effects of the neutrino mass on the CMB, which can be used to break this degeneracy. If neutrinos would exceed the limit $\sum m_\nu \lesssim 1.8$ eV, they would trigger more direct effects in the CMB (Dodelson, Gates & Stebbins 1996; Ichikawa, Fukugita & Kawasaki 2005), which are not observed. This represents probably the most robust limit on the neutrino mass from cosmology. Apart from this there are other, more subtle effects on the CMB anisotropies. Changing the neutrino mass and keeping the redshift of matter-radiation equality fixed will change the low-redshift value of $\Omega_\mathrm{m}h^2$. This will change the angular diameter distance to the last scattering surface, $D_\mathrm{A}(z_*)$. Since such changes can be absorbed by changes in the Hubble parameter there is a (geometric) degeneracy between $\sum m_\nu$ and H_0 in the CMB. Beside the angular diameter distance the neutrino mass also impacts the slope of the CMB power spectrum at low multipoles due to the integrated Sachs–Wolfe (ISW) effect (Lesgourgues & Pastor 2006; Planck Collaboration XIX 2013d). The ISW effect describes the energy change of CMB photons caused by the decay of the gravitational potentials during radiation domination (early ISW effect) or Λ domination (late ISW effect). If instead $\Omega_\mathrm{m}h^2$ is kept fixed when varying the neutrino mass, the redshift of matter-radiation equality will change, which affects the position and amplitude of the acoustic peaks in the CMB power spectrum (for more details see e.g. Lesgourgues & Pastor 2012). Weak gravitational lensing of the CMB photons encodes information about the late-time Universe with the *Planck* kernel peaking at around $z \sim 2$ (Planck Collaboration XVIII 2013c). The lensing deflections are caused by an integrated measure of the matter distribution along the line of sight. Using these additional signals, the CMB data are able to break the $\sum m_\nu$–σ_8 degeneracy to some extent. The remaining degeneracy can be broken by including low-redshift σ_8 measurements from other data sets.

Low-redshift measurements of the clustering amplitude (σ_8) are notoriously difficult, and to some extent require priors from the CMB. Most low-redshift probes which are sensitive to σ_8 require the understanding of non-linear effects and usually carry large systematic uncertainties. In this paper we demonstrate that recent constraints on the growth rate $f\sigma_8$, the baryon acoustic oscillation (BAO) scale $D_\mathrm{V}/r_\mathrm{s}$ and the Alcock–Paczynski effect F_AP from the Baryon Oscillation Spectroscopic Survey (BOSS) are robust against variations of $\sum m_\nu$ in the theoretical template. We also show that the constraint on (Ω_m, σ_8) from the shear correlation function of the weak lensing signal of Canada–France–Hawaii Telescope Lensing Survey (CFHTLenS) is robust against variations of $\sum m_\nu$. We therefore claim that combining CMB data sets with these low-redshift growth of structure measurements provides a reliable approach to break the $\sum m_\nu$–σ_8 degeneracy in the CMB.

This paper is organized as follows. In Section 2 we give a brief summary of the effect of neutrinos on the matter perturbations. In Section 3 we introduce constraints on σ_8 from different data sets. In Section 4 we investigate the robustness of different low-redshift σ_8 constraints, with particular focus on the BOSS growth of structure constraint. In Section 5 we investigate the parameter $\sum m_\nu$ as one approach to relieve the tension between these different data sets. In Section 6 we discuss the cosmological implications of our results, and we conclude in Section 7.

2 BACKGROUND

Here we give a brief overview of the effect of massive neutrinos on the matter perturbations in the Universe. More details can be found in most standard text books (see also Lesgourgues & Pastor 2006, 2012; Lesgourgues et al. 2013).

In the absence of massive neutrinos, density perturbations of cold dark matter (CDM) and baryons grow as

$$\delta_\mathrm{m} \propto \begin{cases} a & \text{during matter domination,} \\ a\,D(a) & \text{during } \Lambda \text{ domination,} \end{cases} \quad (1)$$

where a is the scale factor and $D(a)$ is the growth function. The large thermal velocity of neutrinos leads to a free streaming scale, below which they do not contribute to the matter perturbation growth. During matter or Λ domination the free streaming scale can be approximated by

$$k_\mathrm{FS} = 0.82 \frac{\sqrt{\Omega_\Lambda + \Omega_\mathrm{m}(1+z)^3}}{(1+z)^2} \left(\frac{m_\nu}{1\,\mathrm{eV}}\right) h\,\mathrm{Mpc}^{-1}, \quad (2)$$

where m_ν is the mass of the individual neutrino eigenstates. The matter growth is an interplay between the dilution of matter caused by the expansion of the universe and the growth of perturbations through gravitational collapse. Since neutrinos contribute to the homogeneous expansion through the Friedmann equation but do not contribute to the growth of matter perturbations below the free streaming scale, the overall growth of CDM and baryon perturbations on small scales is suppressed and behaves approximately as

$$\delta_\mathrm{cb} \propto \begin{cases} a^{1-\frac{3}{5}f_\nu} & \text{during matter domination,} \\ [a\,D(a)]^{1-\frac{3}{5}f_\nu} & \text{during } \Lambda \text{ domination,} \end{cases} \quad (3)$$

with $f_\nu = \Omega_\nu/\Omega_\mathrm{m}$ (Bond, Efstathiou & Silk 1980). The total matter perturbations are then given by $\delta_\mathrm{m} = (1 - f_\nu)\delta_\mathrm{cb} + f_\nu\delta_\nu$. The

suppression of matter perturbations on small scales leads to a suppression of the power spectrum, $P = \langle \delta \delta^* \rangle$. In the linear regime this suppression can be approximated by (Hu, Eisenstein & Tegmark 1998)

$$\frac{P^{f_\nu} - P^{f_\nu=0}}{P^{f_\nu=0}} \simeq -8 f_\nu, \quad (4)$$

while on scales larger than the free streaming scale, neutrino perturbations behave like CDM (see also Brandbyge et al. 2008; Viel, Haehnelt & Springel 2010).

The overall normalization of the power spectrum is usually parametrized by σ_8 with $P \propto \sigma_8^2$. The CMB measures the scalar amplitude A_s, which must be extrapolated from the redshift of decoupling $z_* \approx 1100$ to redshift zero to obtain σ_8. The relation between A_s and σ_8 is given by

$$\sigma_8^2(a) \propto A_s \int_0^\infty \mathrm{d}k\, k^2 D^2(a) T^2(k) k^{n_s} W(kR), \quad (5)$$

where $R = 8\,h^{-1}\,\mathrm{Mpc}$, n_s is the scalar spectral index and $W(x) = 3[\sin(x) - x\cos(x)]/x$ is the Fourier transform of the top-hat window function. The growth factor $D(a)$, the primordial power spectrum k^{n_s} and the transfer function $T(k)$ define the power spectrum up to a normalization factor, $P(k, a) \propto D^2(a) k^{n_s} T^2(k)$. Comparing low-redshift σ_8 measurements with the extrapolation of σ_8 from the CMB allows us to measure the damping effect of neutrinos (Takada, Komatsu & Futamase 2006). In this paper we are going to use constraints from galaxy redshift surveys as well as weak lensing. While galaxy surveys measure the galaxy power spectrum, which can be related to the matter power spectrum by the galaxy bias, weak lensing surveys are sensitive to a line-of-sight integral over the matter power spectrum weighted by a lensing kernel.

3 COSMOLOGICAL DATA SETS INCLUDED IN THIS ANALYSIS

Here we introduce the different data sets used in our analysis. We start with the BOSS CMASS sample. BOSS, as part of Sloan Digital Sky Survey-III (SDSS-III; Eisenstein et al. 2011; Dawson et al. 2013), is measuring spectroscopic redshifts of ≈1.5 million galaxies (and 150 000 quasars) using the SDSS multifibre spectrographs (Bolton et al. 2012; Smee et al. 2013). The galaxies are selected from multicolour SDSS imaging (Fukugita et al. 1996; Gunn et al. 1998, 2006; Smith et al. 2002; Doi et al. 2010) and cover a redshift range of $z = 0.15$–0.7, where the survey is split into two samples called LOWZ ($z = 0.15$–0.43) and CMASS ($z = 0.43$–0.7). The CMASS-Data Release 11 (DR11) sample covers 6391 deg^2 in the North Galactic Cap and 2107 deg^2 in the South Galactic Cap; the total area of 8498 deg^2 represents a significant increase from CMASS-Data Release 9 (DR9; Ahn et al. 2012; Anderson et al. 2014a), which covered 3265 deg^2 in total. In this analysis we use the CMASS-DR11 results of Beutler et al. (2014), which includes the measurement of the BAO scale, the Alcock–Paczynski effect and the signal of redshift-space distortions (RSD). Note that we do not include other RSD measurements (e.g. Hawkins et al. 2003; Blake et al. 2011; Beutler et al. 2012; Oka et al. 2014), since the measurement methodology and non-linear modelling are different from the one in Beutler et al. (2014).

We also use results from SDSS-II Data Release 7 (DR7; Abazajian et al. 2009) reported in Mandelbaum et al. (2013), where galaxy–galaxy weak lensing together with galaxy clustering has been used to constrain the dark matter clustering.

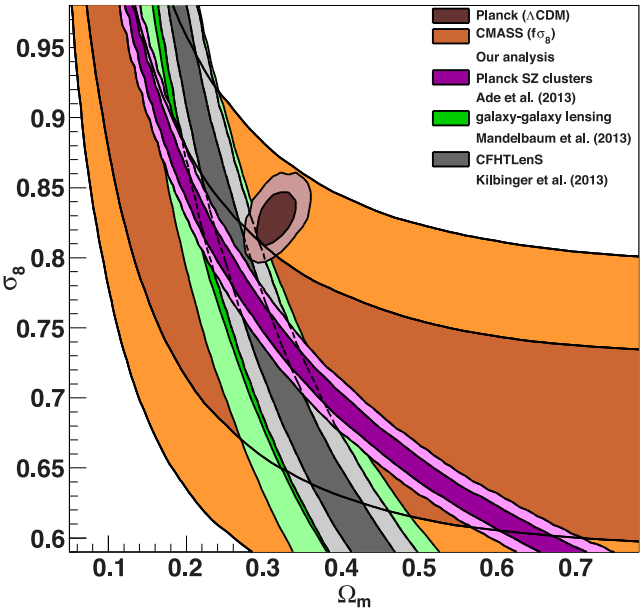

Figure 1. Comparison between the likelihood distributions in Ω_m–σ_8 within ΛCDM. We show *Planck* (Planck Collaboration XVI 2013b) (brown contours), *Planck* SZ clusters (Planck Collaboration XX 2013e) (magenta contours), CFHTLenS (Kilbinger et al. 2013) (grey contours), galaxy–galaxy lensing (Mandelbaum et al. 2013) (green contours) and CMASS-DR11 (Beutler et al. 2014) (orange contours). The *Planck* contours in this plot assume ΛCDM and $\sum m_\nu = 0.06$ eV.

Our second lensing data set is the CFHTLenS (Heymans et al. 2012). The CFHTLenS analysis combined weak lensing data processing with THELI (Erben et al. 2013), shear measurement with lensfit (Miller et al. 2013) and photometric redshift measurement with point spread function (PSF)-matched photometry (Hildebrandt et al. 2012). A full systematic error analysis of the shear measurements in combination with the photometric redshifts is presented in Heymans et al. (2012), with additional error analyses of the photometric redshift measurements presented in Benjamin et al. (2013).

The current most powerful cosmological data sets are measurements of the CMB. We include the 9-year results from the *Wilkinson Microwave Anisotropy Probe* (*WMAP*; Hinshaw et al. 2013) and the first data release of *Planck* (Planck Collaboration XVI 2013b) interchangeably. Both data sets have full-sky, multifrequency coverage and the *Planck* beams are small enough to probe gravitational lensing deflections which was not possible in *WMAP*. We will also compare the original results of *Planck* with the re-analysis by Spergel, Flauger & Hlozek (2013).

In Fig. 1 we present two-dimensional likelihood distributions of Ω_m and σ_8 from the data sets discussed above. Within a flat ΛCDM cosmological model the CMB provides by far the best constraints in this parameter space (brown contours). We show the *Planck*+WP result, which includes the polarization analysis from *WMAP*. The *Planck* prediction of Ω_m and σ_8 relies strongly on the assumption of ΛCDM, since both parameters, Ω_m and σ_8, are extrapolated from information at high redshift. We compare the *Planck* prediction with the lensing result from the CFHTLenS (Kilbinger et al. 2013) (grey contours), the galaxy–galaxy lensing result of Mandelbaum et al. (2013) (green contours) and the result using clusters detected through the Sunyaev–Zel'dovich (SZ) effect in *Planck* (Planck Collaboration XX 2013e) (magenta contours). The orange contours show the CMASS-DR11 results of Beutler et al. (2014) in the form of $f\sigma_8$ (see also Chuang et al. 2013; Samushia et al. 2014;

Sanchez et al. 2014, which gave very similar results). The largest disagreement with the *Planck* prediction comes from the SZ cluster result and has been discussed in Planck Collaboration XX (2013e) [see also Benson et al. 2013 for similar results from South Pole Telescope (SPT)].

4 THE RELIABILITY OF LOW-REDSHIFT GROWTH OF STRUCTURE CONSTRAINTS

We now investigate the reliability of different low-redshift growth of structure measurements with respect to variations of $\sum m_\nu$ in the data modelling process. Low-redshift growth of structure measurements usually reports some combined constraint on Ω_m and σ_8 and assumes a certain value for the neutrino mass when deriving this constraint. To be able to use such a measurement to set limits on the value of the neutrino mass one needs to be sure that the initial assumption about the neutrino mass in the modelling step does not influence the result.

The tightest current constraint comes from SZ clusters detected by *Planck* (Planck Collaboration XX 2013e) in the form

$$\sigma_8 \left(\frac{\Omega_\mathrm{m}}{0.27}\right)^{0.3} = 0.78 \pm 0.01. \quad (6)$$

We include this result as the magenta contours in Fig. 1. The tension between this measurement and the *Planck* temperature power spectrum has been discussed in Planck Collaboration XX (2013e) (see also Battye & Moss 2014; Hamann & Hasenkamp 2013); and including a large value for the sum of the neutrino masses is mentioned as one possibility to relieve this tension. However, Costanzi et al. (2013) showed that in the case of $\sum m_\nu = 0.4$ eV there is up to 30 per cent uncertainty on the predicted cluster count depending on whether the rms of the mass perturbations, $\sigma(M)$, required to predict the halo mass function, is calculated from the CDM power spectrum or the matter power spectrum. In the case of the *Planck* SZ cluster analysis the systematic uncertainty on σ_8 from these effects is twice as large as the statistical error reported by the *Planck* collaboration. Cluster counts also carry an uncertainty from the unknown bias in the mass–observable relations (Rozo et al. 2013; von der Linden et al. 2014). Because of these uncertainties we will not include the SZ cluster results in the parameter constraints in this paper.

4.1 Reliability of the CMASS constraints

In Beutler et al. (2014) we analysed the CMASS power spectrum multipoles and constrained the distance ratio $D_\mathrm{V}/r_\mathrm{s}(z_\mathrm{d})$, where $r_\mathrm{s}(z_\mathrm{d})$ is the sound horizon at the drag epoch, and

$$D_\mathrm{V} = \left[(1+z)^2 D_\mathrm{A}^2(z) \frac{cz}{H(z)}\right]^{1/3}, \quad (7)$$

as well as the Alcock–Paczynski parameter $F_\mathrm{AP} = (1+z)D_\mathrm{A}(z)H(z)/c$ and the growth of structure $f\sigma_8$. Our technique made use of a power spectrum template, based on the current *Planck* cosmological parameters including several non-linear effects which are parametrized by four nuisance parameters. We scaled this template with two scaling parameters, $\alpha_\parallel$ and $\alpha_\perp$, along with the RSD parameter $f\sigma_8$. We performed several systematics tests, which demonstrated that the power spectrum can be used up to $k = 0.20\,h\,\mathrm{Mpc}^{-1}$, where our constraints are still dominated by the statistical error. To some extent our technique must be understood as a consistency check within the *Planck* cosmological parameters, since we rely on the *Planck* power spectrum template. However, as shown in Beutler et al. (2014), the parameter constraints do not rely heavily on the template itself. For example, we can replace the *Planck* template with a *WMAP*9 template and not bias our parameter constraints (see Beutler et al. 2014, section 7 for details). Another systematics check has been performed in Ross et al. (2014), where we showed that the BAO and RSD constraints are independent of different colour cuts within the CMASS data set.

The question we want to address here is, what happens when we introduce a neutrino mass in the power spectrum template? The power spectrum template in Beutler et al. (2014) assumes $\sum m_\nu = 0$ eV. The neutrino mass introduces a scale-dependent damping in the power spectrum. Since our analysis includes four nuisance parameters to capture scale dependencies, we can expect that some of the changes in the power spectrum template will be absorbed by these nuisance parameters.

To explicitly test the effect of the neutrino mass we produce a linear power spectrum using CAMB (Lewis & Bridle 2002) setting the neutrino mass parameter to $\sum m_\nu = 0.4$ eV with three massive neutrinos with degenerate masses. We keep $\Omega_\mathrm{c}\,h^2$ fixed when including the neutrino mass, so that the total physical matter density increases as $\Omega_\mathrm{m}\,h^2 = \Omega_\mathrm{c}\,h^2 + \Omega_\mathrm{b}\,h^2 + \Omega_\nu\,h^2$. The physical neutrino density is given by

$$\Omega_\nu\,h^2 = \frac{\sum m_\nu}{93.14\,\mathrm{eV}}. \quad (8)$$

We use the linear matter power spectrum as input for the non-linear power spectrum produced via REGPT (Taruya et al. 2012) as well as the correction terms summarized in section 6 of Beutler et al. (2014). Strictly speaking, REGPT is not designed to include the non-linear clustering contribution of neutrinos. By using the linear matter power spectrum as an input to REGPT we assume that non-linear corrections for the matter power spectrum are identical for neutrinos, CDM and baryons. This assumption is incorrect, since neutrino perturbations tend to stay in the linear regime even where non-linear corrections to the matter power spectrum are not negligible (Saito, Takada & Taruya 2008, 2009; Wong 2008). However, these effects are small on the scales we are interested in and should not influence the outcome of this test. The difference between the linear matter power spectrum multipoles with a neutrino mass parameter of $\sum m_\nu = 0.4$ eV and zero neutrino mass is shown in Fig. 2.

Also notice that a non-zero neutrino mass introduces a scale dependence in the growth rate $f(k, a) = \mathrm{d}\ln D(k, a)/\mathrm{d}\ln a$ as shown in Fig. 3. To compare with the CMB prediction of the growth rate we desire to know the value $f(k \to 0)$ instead of some effective growth rate. In the case of $\sum m_\nu = 0.4$ eV the suppression is 1.4 per cent at $k = 0.20\,h\,\mathrm{Mpc}^{-1}$. We include this effect in our parameter fit, by using $f\sigma_8 g(k)$ as a free parameter instead of $f\sigma_8$, where

$$g(k) = \frac{f(z, \sum m_\nu = 0.4\,\mathrm{eV})}{f(z, \sum m_\nu = 0\,\mathrm{eV})}. \quad (9)$$

Using the new power spectrum template we repeat the parameter fit of Beutler et al. (2014) with the fitting range $k = 0.01$–$0.20\,h\,\mathrm{Mpc}^{-1}$. Table 1 and Fig. 4 (left) summarize the results. The new template is a slightly worse fit to the data set compared to the template with $\sum m_\nu = 0$ eV used in Beutler et al. (2014), since the χ^2 increases by $\Delta\chi^2 = 7.6$ to $\chi^2/\mathrm{d.o.f.} = 148.1/145$. This degradation is also reflected in the increased error bars for some parameters. However, this result cannot be interpreted as preference for zero neutrino mass, since all other cosmological parameters in the power spectrum template were fixed. The best-fitting values show shifts $<0.5\sigma$ for the three cosmological parameters. As expected, the BAO scale is

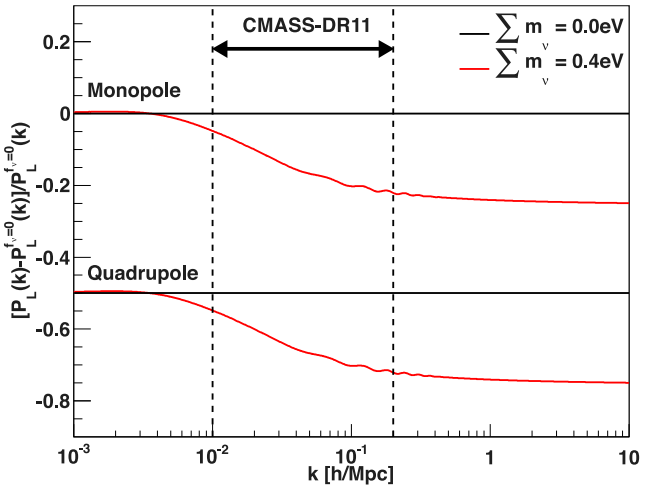

Figure 2. Relative amplitude difference between a linear power spectrum monopole (top) and quadrupole (bottom) with $\sum m_\nu = 0$ eV (black lines) and $\sum m_\nu = 0.4$ eV (red lines). We keep $\Omega_c\,h^2$ fixed when including the neutrino mass, so that the total physical matter density increases as $\Omega_m\,h^2 = \Omega_c\,h^2 + \Omega_b\,h^2 + \Omega_\nu\,h^2$. The black dashed lines show the fitting range for the CMASS-DR11 results of Beutler et al. (2014). We subtract 0.5 from the quadrupole for plotting purposes.

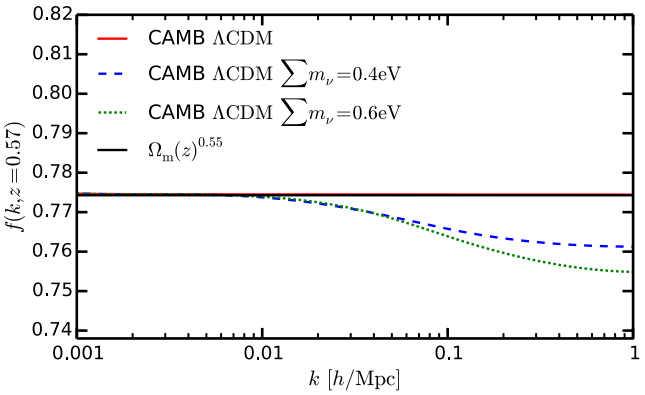

Figure 3. Scale dependence of the growth rate for different values of the neutrino mass parameter. The black line shows the commonly used linear assumption, while all other lines are obtained as derivatives of the growth factor $D(k, a)$ using a CAMB power spectrum. In this figure we fix $\Omega_m\,h^2$ when increasing the neutrino mass.

very robust against changes in the template, while we see larger shifts in F_{AP} and $f\sigma_8$ (see Fig. 4, left). Since F_{AP} and $f\sigma_8$ are correlated the significance of this shift is lower when accounting for the correlation. We calculate the quantity

$$\Delta\chi^2_{dif} = (V^{data}_{f_\nu} - V^{data}_{f_\nu=0})^T \mathbf{C}^{-1} (V^{data}_{f_\nu} - V^{data}_{f_\nu=0}), \quad (10)$$

where $V^{data}_{f_\nu}$ is the data vector of D_V/r_s, F_{AP} and $f\sigma_8$, derived in this paper and $V^{data}_{f_\nu=0}$ stands for the equivalent results of Beutler et al. (2014). We use the covariance matrix, $\mathbf{C}^{-1}$, reported in equation (72) of Beutler et al. (2014). For the values in Table 1 we find $\Delta\chi^2_{dif} = 0.29$ with three degrees of freedom. While the shifts reported in Table 1 do not seem significant, they lead to smaller $f\sigma_8$ which would increase the preference for a neutrino mass, as discussed in the next section. These possible systematics are of the same order as the modelling systematics discussed in Beutler et al. (2014), which when treated as independent error contributions increase the total error budged by 5 per cent. We conclude that our cosmological parameter constraints are robust against changes in the power spectrum template related to the neutrino mass.

4.2 Reliability of the CFHTLenS constraint

Now we test the reliability of the CFHTLenS results when changing the neutrino mass parameter in the shear–shear correlation function model. We use the Population Monte Carlo code CosmoPMC (Kilbinger et al. 2011), which was also used for the CFHTLenS analysis in Kilbinger et al. (2013). CosmoPMC uses the linear matter power spectrum fitting formula of Eisenstein & Hu (1998) when modelling the shear–shear correlation function as well as the HALOFIT mapping of Smith et al. (2003), neither of which includes the effect of massive neutrinos. We therefore modify the code by including the linear power spectrum fitting formula of Eisenstein & Hu (1999) and the HALOFIT mapping suggested in Bird et al. (2012). The HALOFIT implementation of Bird et al. (2012) also includes a correction to the power spectrum amplitude on small scales, which Smith et al. (2003) overpredict. The effect of this correction to the CFHTLenS constraints is shown in Fig. 4 (right), where the black contours use the HALOFIT mapping of Smith et al. (2003), while the blue contours use the HALOFIT mapping of Bird et al. (2012). If we also include a neutrino mass of $\sum m_\nu = 0.4$ eV we obtain the red contours. At $\Omega_m = 0.3$ the difference between black and the blue contours is $\sim 1\sigma$ for σ_8. When introducing a neutrino mass (red contours) there is another shift of $\sim\sigma/3$. We therefore conclude that while the CFHTLenS constraint shows some sensitivity to the exact treatment of non-linear clustering, it does not seem to be very sensitive

Table 1. Comparison between the best fitting and mean parameters of Beutler et al. (2014) and the results obtained in this paper, where $\sum m_\nu = 0.4$ eV has been used in the power spectrum template. The first three rows show the main cosmological parameters, while the last four rows show the four nuisance parameters of the fit. The fitting range is $k = 0.01$–$0.20\,h\,\mathrm{Mpc}^{-1}$. Details about the modelling can be found in Beutler et al. (2014).

	Beutler et al. (2013)		Template with $\sum m_\nu = 0.4$ eV	
Parameter	Best fit	Mean	Best fit	Mean
$D_V(z_{eff})/r_s(z_d)$	13.88	13.89 ± 0.18	13.87	13.91 ± 0.25
$F_{AP}(z_{eff})$	0.683	0.679 ± 0.031	0.664	0.664 ± 0.035
$f(z_{eff})\sigma_8(z_{eff})$	0.422	0.419 ± 0.044	0.404	0.405 ± 0.048
$b_1\sigma_8(z_{eff})$	1.221	1.224 ± 0.031	1.183	1.188 ± 0.039
$b_2\sigma_8(z_{eff})$	−0.21	-0.09 ± 0.62	−0.67	-0.72 ± 0.41
σ_v	4.63 Mpc h^{-1}	4.65 ± 0.81 Mpc h^{-1}	4.9 Mpc h^{-1}	4.9 ± 1.0 Mpc h^{-1}
N	1890 [Mpc h^{-1}]^3	1690 ± 600 [Mpc h^{-1}]^3	3400 [Mpc h^{-1}]^3	3400 ± 1100 [Mpc h^{-1}]^3

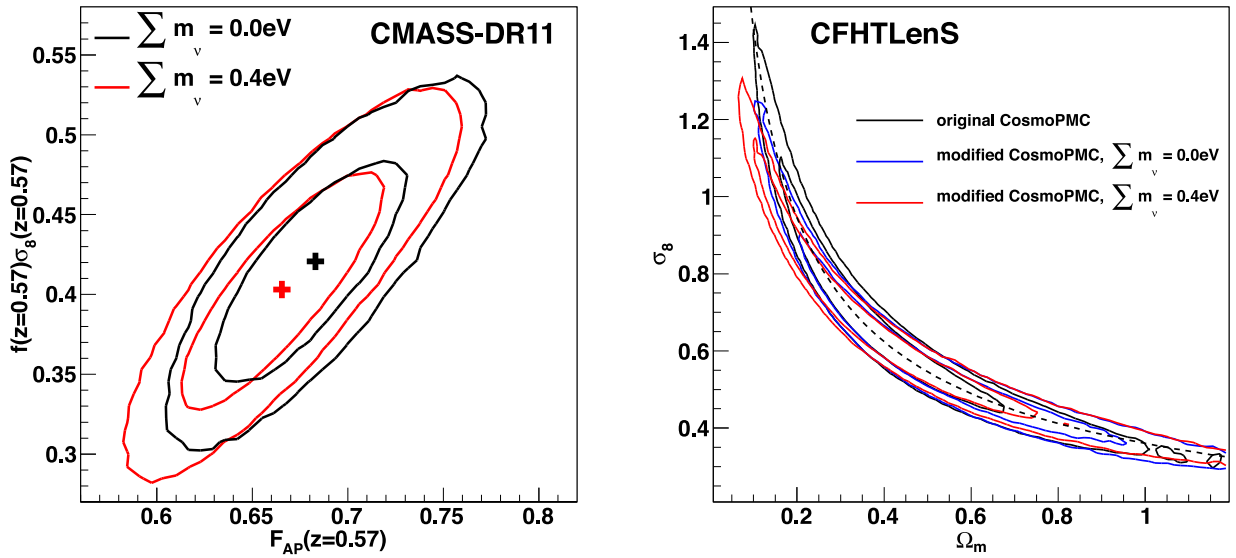

Figure 4. Results of the reliability tests for the CMASS and CFHTLenS constraints. The red contours include a neutrino mass of $\sum m_\nu = 0.4$ eV in the modelling, while the black contours assume $\sum m_\nu = 0$ eV. Left: here we show the Alcock–Paczynski parameter $F_{\rm AP}$ and the growth rate $f\sigma_8$ from CMASS-DR11, which are the two parameters most affected by the change in the neutrino mass parameter (in the analysis we also include the BAO scale via $D_{\rm V}/r_{\rm s}$). The crosses mark the maximum likelihood values. Right: here we show the $\Omega_{\rm m}$–σ_8 constraints of CFHTLenS including the degeneracy line used in our analysis and reported in Kilbinger et al. (2013) (black dashed line). The black contours show the original fitting results using the CosmoPMC implementation of Kilbinger et al. (2011), while the blue contours use a modified code with the biggest difference being the new HALOFIT implementation of Bird, Viel & Haehnelt (2012) (see text for details).

to the effect of the neutrino mass. Note that all shifts shown in Fig. 4 (right) lead to a smaller clustering amplitude (at fixed $\Omega_{\rm m}$) and therefore would increase the preference for neutrino mass (see next section).

Here we are not explicitly testing the reliability of the galaxy–galaxy lensing result of Mandelbaum et al. (2013) which we are also going to use later in this analysis, but refer the reader to section 2.3.2 in Mandelbaum et al. (2013).

5 CONSTRAINING THE MASS OF NEUTRINOS

Knowing that our CMASS measurements and the weak lensing constraints are quite insensitive to the fiducial neutrino mass we now combine these constraints with CMB data from *WMAP*9[1] and *Planck*.[2] We importance sample the CMB Markov chain Monte Carlo (MCMC) chains, where $\sum m_\nu$ is varied freely. Importance sampling means that we adjust the weight of each chain element in the original CMB chain by the likelihood, $\mathcal{L} \sim \exp(-\chi^2/2)$, of some external data set, according to

$$w_{\rm new} = w_{\rm CMB}\,\mathcal{L}. \tag{11}$$

The distribution of these new weights reflects the combined likelihood.

To provide constraints on some combination of σ_8 and $\Omega_{\rm m}$ we adopted the CMASS $f\sigma_8$ measurement of Beutler et al. (2014), the CFHTLenS constraint reported in Kilbinger et al. (2013),

$$\sigma_8 \left(\frac{\Omega_{\rm m}}{0.27}\right)^{0.6} = 0.79 \pm 0.03, \tag{12}$$

and the galaxy–galaxy lensing result reported in Mandelbaum et al. (2013),

$$\sigma_8 \left(\frac{\Omega_{\rm m}}{0.25}\right)^{0.57} = 0.80 \pm 0.05. \tag{13}$$

We prefer to use the full degeneracy lines (equations 12 and 13) from these lensing results instead of the actual likelihoods. This approach is more conservative and does not affect our final results given the power of the BAO scale to break the degeneracy between $\Omega_{\rm m}$ and σ_8. We occasionally also include the BAO constraint of 6dF Galaxy Survey (6dFGS; Beutler et al. 2011) and LOWZ (Anderson et al. 2014b; Tojeiro et al. 2014). In Section 6 we will discuss the significance with which these data sets prefer ΛCDM+$\sum m_\nu$ over ΛCDM.

5.1 Combining with *WMAP*9

We start with importance sampling the *WMAP*9 chains.[3] To illustrate the constraining power of the different data sets we use them one by one, before combining them. These results are summarized in Table 2 and shown in Figs 5 and 6. Using *WMAP*9 alone already allows a constraint on $\sum m_\nu$ of <1.3 eV with 95 per cent confidence level. If we add BAO constraints, where we use the isotropic CMASS constraint after density field reconstruction from Anderson et al. (2014b) (Anderson2013b), we obtain an upper limit of <0.54 eV with 95 per cent confidence level. Therefore adding current BAO information already improves the constraint by more than a factor of 2. The CMB combined with BAO constrain the neutrino mass purely from its effect on the geometry of the Universe, with the BAO particularly helping to break the degeneracy between $\sum m_\nu$ and H_0 (see e.g. Hou et al. 2014).

[1] http://lambda.gsfc.nasa.gov/product/map/current/
[2] http://irsa.ipac.caltech.edu/data/Planck/release_1/ancillary-data/
[3] http://lambda.gsfc.nasa.gov/product/map/current/

Table 2. Constraints on σ_8, Ω_m and $\sum m_\nu$ combining different data sets. The errors on σ_8 and Ω_m are 1σ, while for $\sum m_\nu$ we report the 68 and 95 per cent confidence levels. *Planck* stands for the *Planck*+WP result reported in Planck Collaboration XVI (2013b), *WMAP*9 represents the 9-year results of *WMAP* reported in Hinshaw et al. (2013), Spergel2013 stands for the *Planck* re-analysis of Spergel et al. (2013), Beutler2013 represents the constraints on D_V/r_s, F_{AP} and $f\sigma_8$ from Beutler et al. (2014), CFHTLenS represents the weak lensing results from Kilbinger et al. (2013), GGlensing represents the galaxy–galaxy lensing results reported in Mandelbaum et al. (2013) and BAO stands for the BAO constraint of 6dFGS (Beutler et al. 2011) and the isotropic BAO constraints of LOWZ (Anderson et al. 2014b; Tojeiro et al. 2014). We also include the CMB lensing result from the four-point function (CMBlensing) reported by the *Planck* collaboration (Planck Collaboration XVIII 2013c). In some cases we replace the results of Beutler et al. (2014) (Beutler2013) with Samushia et al. (2014) (Samushia2013), Chuang et al. (2013) (Chaung2013) and the BAO only constraints of Anderson et al. (2014b) (Anderson2013b). In the cases of Beutler2013, Samushia2013 and Chaung2013 we make use of the covariance matrix between the three constraints (D_V/r_s, F_{AP} and $f\sigma_8$) presented in the corresponding papers. We also include results using the *Planck* MCMC chains where the lensing effect on the temperature power spectrum (A_L lensing) has been marginalized out (*Planck*–A_L). The *Planck*, *Planck*–A_L and Spergel2013 chains include polarization results from *WMAP* (WP).

Data set(s)	σ_8	Ω_m	$\sum m_\nu$ (eV)	
			68 per cent c.l.	95 per cent c.l.
*WMAP*9	0.706 ± 0.077	$0.354^{+0.048}_{-0.078}$	<0.75	<1.3
*WMAP*9+CFHTLenS	$0.696^{+0.094}_{-0.071}$	$0.343^{+0.046}_{-0.078}$	<0.76	<1.3
*WMAP*9+Beutler2013	0.733 ± 0.038	0.309 ± 0.015	0.36 ± 0.14	0.36 ± 0.28
*WMAP*9+Beutler2013+CFHTLenS	0.731 ± 0.026	0.308 ± 0.014	0.37 ± 0.12	0.37 ± 0.24
*WMAP*9+Beutler2013+GGlensing	0.725 ± 0.029	0.307 ± 0.014	0.39 ± 0.12	0.39 ± 0.25
*WMAP*9+Beutler2013+CFHTLenS+GGlensing+BAO	0.733 ± 0.024	0.303 ± 0.011	0.35 ± 0.10	0.35 ± 0.21
*WMAP*9+Samushia2013	0.746 ± 0.036	0.303 ± 0.013	0.31 ± 0.13	0.31 ± 0.25
*WMAP*9+Samushia2013+CFHTLenS+GGlensing+BAO	0.740 ± 0.023	0.2991 ± 0.0097	0.32 ± 0.10	0.32 ± 0.20
*WMAP*9+Chuang2013	0.717 ± 0.046	0.311 ± 0.015	0.42 ± 0.17	0.42 ± 0.35
*WMAP*9+Chuang2013+CFHTLenS+GGlensing+BAO	0.728 ± 0.026	0.304 ± 0.011	0.36 ± 0.11	0.36 ± 0.23
*WMAP*9+Anderson2013	$0.763^{+0.058}_{-0.040}$	0.295 ± 0.011	<0.31	<0.54
*WMAP*9+Anderson2013+BAO	$0.763^{+0.060}_{-0.041}$	0.2946 ± 0.0093	<0.31	<0.53
*WMAP*9+Anderson2013+CFHTLenS+GGlensing+BAO	0.750 ± 0.029	0.2936 ± 0.0097	0.27 ± 0.12	0.27 ± 0.22
Planck	$0.775^{+0.074}_{-0.031}$	$0.353^{+0.021}_{-0.058}$	<0.41	<0.95
Planck+CFHTLenS	$0.745^{+0.083}_{-0.112}$	0.332 ± 0.064	<0.51	<1.0
Planck+Beutler2013	$0.791^{+0.034}_{-0.025}$	0.320 ± 0.014	0.20 ± 0.13	<0.40
Planck+Beutler2013+CFHTLenS	$0.760^{+0.026}_{-0.047}$	0.314 ± 0.019	0.29 ± 0.13	$0.29^{+0.29}_{-0.23}$
Planck+Beutler2013+GGlensing	0.769 ± 0.035	0.316 ± 0.016	0.26 ± 0.13	0.26 ± 0.24
Planck+Beutler2013+CFHTLenS+GGlensing+BAO	$0.759^{+0.025}_{-0.033}$	0.306 ± 0.015	0.27 ± 0.12	0.27 ± 0.21
Planck+CMBlensing+Beutler2013+CFHTLenS+GGlensing+BAO	$0.774^{+0.025}_{-0.037}$	0.304 ± 0.014	0.24 ± 0.14	0.24 ± 0.20
Planck+Samushia2013	$0.800^{+0.029}_{-0.023}$	0.315 ± 0.013	$0.161^{+0.068}_{-0.139}$	<0.33
Planck+Samushia2013+CFHTLenS+GGlensing+BAO	0.765 ± 0.031	0.303 ± 0.014	$0.243^{+0.132}_{-0.088}$	0.24 ± 0.19
Planck+Chuang2013	$0.797^{+0.038}_{-0.026}$	0.319 ± 0.014	<0.23	<0.40
Planck+Chuang2013+CFHTLenS+GGlensing+BAO	$0.759^{+0.027}_{-0.037}$	0.306 ± 0.015	0.27 ± 0.12	0.27 ± 0.22
Planck+Anderson2013	$0.821^{+0.023}_{-0.012}$	0.304 ± 0.010	<0.10	<0.22
Planck+Anderson2013+BAO	$0.821^{+0.022}_{-0.013}$	0.3020 ± 0.0084	<0.09	<0.21
Planck+Anderson2013+CFHTLenS+GGlensing+BAO	$0.782^{+0.029}_{-0.048}$	$0.296^{+0.010}_{-0.015}$	0.17 ± 0.12	<0.33
Planck+CMBlensing+Anderson2013+CFHTLenS+GGlensing+BAO	$0.794^{+0.025}_{-0.032}$	0.294 ± 0.012	$0.15^{+0.15}_{-0.12}$	<0.30
Planck+CMBlensing	$0.746^{+0.086}_{-0.038}$	$0.373^{+0.048}_{-0.077}$	<0.62	<1.1
Planck $-$ A_L	$0.716^{+0.092}_{-0.064}$	$0.356^{+0.043}_{-0.065}$	<0.71	<1.2
Planck $-$ A_L+CFHTLenS	$0.694^{+0.099}_{-0.079}$	$0.351^{+0.048}_{-0.076}$	$0.62^{+0.36}_{-0.50}$	<1.3
Planck $-$ A_L+Beutler2013	0.746 ± 0.035	0.316 ± 0.015	0.34 ± 0.14	0.34 ± 0.26
Planck $-$ A_L+Beutler2013+CFHTLenS	0.733 ± 0.027	$0.314^{+0.013}_{-0.018}$	0.38 ± 0.11	0.38 ± 0.24
Planck $-$ A_L+Beutler2013+GGlensing	0.733 ± 0.031	$0.314^{+0.013}_{-0.017}$	0.38 ± 0.12	0.38 ± 0.25
Planck $-$ A_L+Beutler2013+CFHTLenS+GGlensing+BAO	0.736 ± 0.024	0.307 ± 0.011	0.36 ± 0.10	0.36 ± 0.21
Planck $-$ A_L+CMBlensing+Beutler2013+CFHTLenS+GGlensing+BAO	$0.731^{+0.030}_{-0.040}$	0.309 ± 0.015	$0.38^{+0.12}_{-0.17}$	0.38 ± 0.20
Planck $-$ A_L+Samushia2013	0.759 ± 0.035	0.310 ± 0.013	0.28 ± 0.12	0.28 ± 0.23
Planck $-$ A_L+Samushia2013+CFHTLenS+GGlensing+BAO	0.743 ± 0.024	0.303 ± 0.011	0.324 ± 0.099	0.32 ± 0.19
Planck $-$ A_L+Chuang2013	0.737 ± 0.042	0.318 ± 0.016	$0.38^{+0.15}_{-0.19}$	0.38 ± 0.32
Planck $-$ A_L+Chuang2013+CFHTLenS+GGlensing+BAO	0.730 ± 0.028	0.309 ± 0.012	0.38 ± 0.11	0.38 ± 0.22
Planck $-$ A_L+Anderson2013	$0.784^{+0.046}_{-0.026}$	$0.299^{+0.010}_{-0.013}$	<0.23	<0.43

Table 2 *continued*

Data set(s)	σ_8	Ω_m	$\sum m_\nu$ (eV) 68 per cent c.l.	$\sum m_\nu$ (eV) 95 per cent c.l.
Planck $-A_L$+Anderson2013+BAO	$0.785^{+0.046}_{-0.029}$	0.2985 ± 0.0094	<0.23	<0.42
Planck $-A_L$+Anderson2013+CFHTLenS+GGlensing+BAO	0.755 ± 0.028	0.297 ± 0.010	0.27 ± 0.11	0.27 ± 0.21
Planck $-A_L$+CMBlensing+Anderson2013+CFHTLenS+GGlensing+BAO	0.747 ± 0.036	0.300 ± 0.014	0.30 ± 0.15	0.30 ± 0.24
Planck $-A_L$+CMBlensing	$0.658^{+0.036}_{-0.062}$	$0.400^{+0.066}_{-0.051}$	$0.86^{+0.35}_{-0.28}$	0.86 ± 0.67
Spergel2013	$0.761^{+0.074}_{-0.033}$	$0.343^{+0.024}_{-0.056}$	<0.44	<0.92
Spergel2013+CFHTLenS	$0.741^{+0.077}_{-0.058}$	$0.329^{+0.034}_{-0.058}$	<0.50	<0.99
Spergel2013+Beutler2013	0.774 ± 0.029	0.317 ± 0.015	0.24 ± 0.12	0.24 ± 0.22
Spergel2013+Beutler2013+CFHTLenS	$0.753^{+0.025}_{-0.032}$	0.313 ± 0.016	0.30 ± 0.11	0.30 ± 0.23
Spergel2013+Beutler2013+GGlensing	$0.758^{+0.029}_{-0.037}$	0.314 ± 0.015	0.29 ± 0.12	0.29 ± 0.23
Spergel2013+Beutler2013+CFHTLenS+GGlensing+BAO	$0.754^{+0.024}_{-0.033}$	0.306 ± 0.011	0.29 ± 0.10	0.29 ± 0.20
Spergel2013+Samushia2013	0.784 ± 0.028	0.312 ± 0.013	$0.201^{+0.091}_{-0.113}$	<0.38
Spergel2013+Samushia2013+CFHTLenS+GGlensing+BAO	0.760 ± 0.024	0.303 ± 0.011	0.26 ± 0.10	0.26 ± 0.19
Spergel2013+Chuang2013	0.777 ± 0.034	0.317 ± 0.016	$0.24^{+0.11}_{-0.15}$	<0.47
Spergel2013+Chuang2013+CFHTLenS+GGlensing+BAO	$0.752^{+0.025}_{-0.032}$	0.307 ± 0.011	0.29 ± 0.11	0.29 ± 0.22
Spergel2013+Anderson2013	$0.807^{+0.028}_{-0.016}$	0.300 ± 0.011	<0.14	<0.27
Spergel2013+Anderson2013+BAO	$0.808^{+0.027}_{-0.015}$	0.2992 ± 0.0086	<0.13	<0.26
Spergel2013+Anderson2013+CFHTLenS+GGlensing+BAO	0.776 ± 0.027	0.296 ± 0.010	$0.191^{+0.098}_{-0.122}$	<0.36

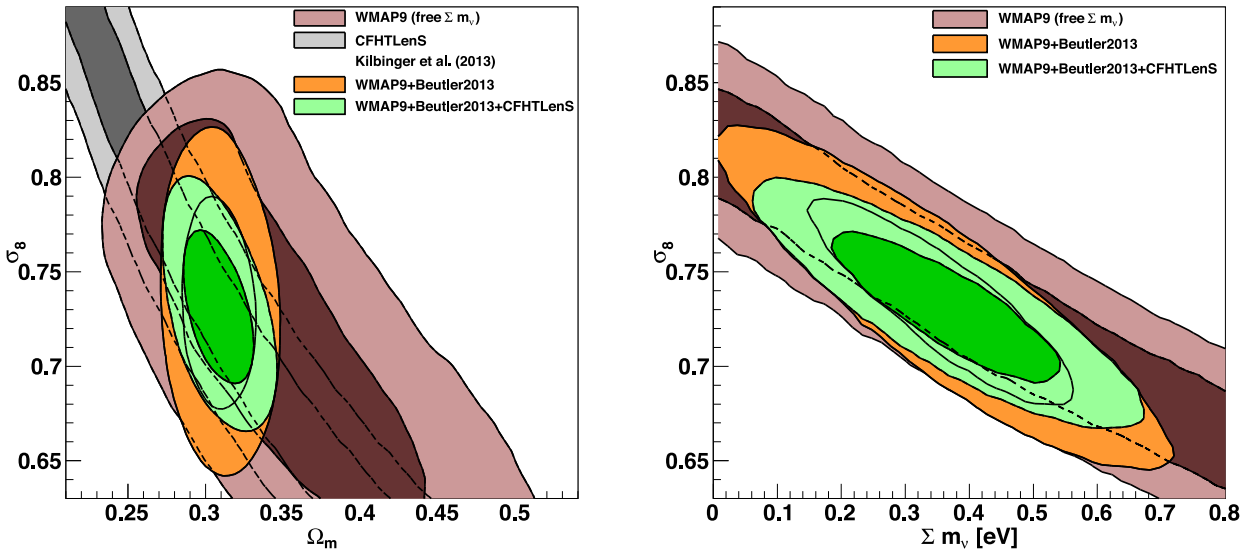

Figure 5. Two-dimensional likelihood for Ω_m–σ_8 (left) and $\sum m_\nu$–σ_8 (right) when combining the *WMAP*9 MCMC chain within ΛCDM and free $\sum m_\nu$ with different low-redshift growth of structure constraints. The orange contours show *WMAP*9+Beutler2013, where Beutler2013 stands for the constraints on D_V/r_s, F_{AP} and $f\sigma_8$ reported in Beutler et al. (2014). The green contours show *WMAP*9+Beutler2013+CFHTLenS. The results are summarized in Table 2.

Next we use the lensing results from CFHTLenS (Kilbinger et al. 2013) and galaxy–galaxy lensing (Mandelbaum et al. 2013) (GGlensing). The degeneracy lines in these lensing results are similar to the degeneracy in the CMB and therefore combining *WMAP*9 with only weak lensing measurements does not improve the neutrino mass constraint significantly (see Table 2 for details). The true power of the lensing data sets arises with the addition of the BAO information. The BAO constraints basically fix Ω_m, which, combined with weak lensing, allows tight constraints on σ_8. These σ_8 constraints are almost a factor of 2 better than CMB+BAO and improve the neutrino mass constraint significantly. The same arguments hold for the $f\sigma_8$ constraint from galaxy surveys. Since one can obtain both, the BAO scale measurement and the growth of structure measurement from galaxy surveys, we can combine just two data sets, *WMAP*9 and CMASS, to obtain tight constraints on the neutrino mass. Combining the CMASS-DR11 results for D_V/r_s, F_{AP} and $f\sigma_8$ reported in equations (68) and (70) of Beutler et al. (2014) with *WMAP*9 produces $\sum m_\nu = 0.36 \pm 0.14$ eV, which represents a 2.6σ preference for neutrino mass. Adding CFHTLenS further improves this constraint to $\sum m_\nu = 0.37 \pm 0.12$ eV, which represents a 3.1σ detection. Replacing CFHTLenS with galaxy–galaxy lensing from Mandelbaum et al. (2013) (GGlensing) leads to basically the same result. Combining all data sets, including further BAO constraints from 6dFGS and LOWZ, yields $\sum m_\nu = 0.35 \pm 0.10$ eV (3.3σ).

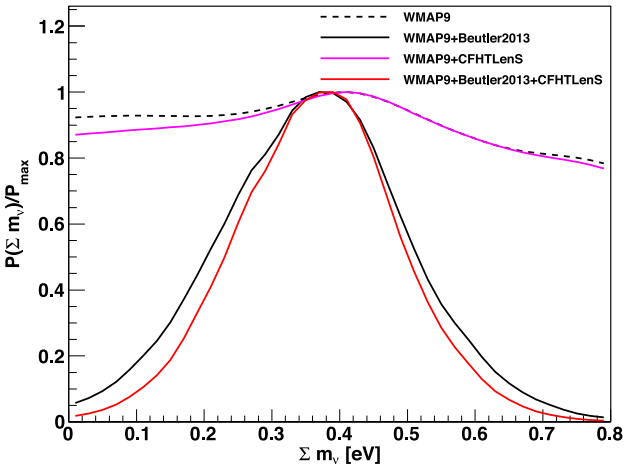

Figure 6. One-dimensional likelihood distribution for $\sum m_\nu$ using *WMAP*9 combined with different data sets. Beutler2013 stands for the D_V/r_s, F_{AP} and $f\sigma_8$ constraints of Beutler et al. (2014), while CFHTLenS represents the constraint of equation (12) reported in Kilbinger et al. (2013) (see also Table 2).

The final result does not change significantly if we use the constraints of Samushia et al. (2014) (Samushia2013b), Chuang et al. (2013) (Chuang2013) or the BAO-only constraints of Anderson et al. (2014b) (Anderson2013b) instead of Beutler et al. (2014).

5.2 Combining with *Planck*

We now replace the *WMAP*9 data set with *Planck*[4] and repeat the exercise of the last section. The results are summarized in Table 2 and shown in Figs 7 (upper two plots) and 8 (top). Combining *Planck* with the results of Beutler et al. (2014) yields a mild preference for neutrino mass of $\sum m_\nu = 0.20 \pm 0.13$ eV (68 per cent c.l.) or an upper limit of <0.40 eV with 95 per cent confidence level. Including CFHTLenS produces $\sum m_\nu = 0.29 \pm 0.13$ eV. Adding galaxy–galaxy lensing or further BAO measurements results in a 2.3σ preference of neutrino mass yielding $\sum m_\nu = 0.27 \pm 0.12$ eV. When replacing the result of Beutler et al. (2014) with Samushia et al. (2014), Chuang et al. (2013) or Anderson et al. (2014b) we find consistent results. Note that since *Planck* is in tension with some of the other data sets, importance sampling does rely on fairly low-density regions in the *Planck* chains. We conclude that these results cannot be used to claim a significant detection of the neutrino mass.

5.3 Combining with *Planck* marginalized over A_L

Table 2 also includes results using *Planck* MCMC chains where the lensing contribution to the temperature power spectrum has been marginalized out. We denote this chain *Planck*–A_L since A_L is the parameter used to mimic the lensing effect on the CMB temperature power spectrum (smoothing of the higher order peaks). One must keep in mind, however, that A_L is not a physical parameter, but only a way to remove the lensing effect from the CMB power spectrum data. To avoid confusion, from now on we will designate the lensing contribution to the temperature power spectrum as A_L lensing and the lensing signal in the four-point function as CMB lensing (or CMBlensing in Table 2). The *WMAP* data set is not sensitive to gravitational lensing, because this effect is only significant at large multipoles.

The *Planck* collaboration reports some anomalies with respect to the A_L lensing contribution. When including the parameter A_L in the fit, *Planck* reports $A_L = 1.29 \pm 0.13$ (*Planck*+WP) (Planck Collaboration XVI 2013b), which is 2σ from the expected value of 1, while the lensing effect in the four-point function produces $A_L^{\phi\phi} = 0.99 \pm 0.05$ (Planck Collaboration XVIII 2013c). Thus the A_L lensing contribution is in (small) tension with the overall *Planck* results and with the four-point function lensing of *Planck*. The CMB lensing of *Planck* favours larger neutrino masses compared to the rest of *Planck*, which therefore leads to a weakening of the neutrino mass constraints when CMB lensing is included (see Planck Collaboration XVI 2013b, section 6.3.1). We show these results in Table 2, where *Planck*+WP gives $\sum m_\nu < 0.95$ eV, while *Planck*+WP+CMBlensing yields $\sum m_\nu < 1.1$ eV. While the neutrino mass constraints improve if Atacama Cosmology Telescope (ACT; Das et al. 2014) and SPT (Keisler et al. 2011) data (highL) are included, it does not relieve the tensions with A_L lensing. Because of the points mention above it is interesting to investigate what happens with the *Planck* data when the A_L lensing signal is excluded.

Excluding the A_L lensing contribution significantly degrades the constraints on the neutrino mass from *Planck* alone, since these constraints are dominated by the A_L lensing effect. This, however, has little effect on our analysis, since we can break the $\sum m_\nu$–σ_8 degeneracy more efficiently with the low-redshift data sets. Another effect of marginalizing over A_L is much more significant. Marginalizing over A_L leads to 1σ shifts in Ω_m and σ_8. Within ΛCDM including the default value of $\sum m_\nu = 0.06$ eV, the *Planck* team found for Ω_m:

$$\Omega_m = 0.315^{+0.016}_{-0.018} \qquad (Planck + \mathrm{WP}), \tag{14}$$

$$\Omega_m = 0.295^{+0.017}_{-0.020} \qquad (Planck\text{-}A_L + \mathrm{WP}), \tag{15}$$

and for σ_8:

$$\sigma_8 = 0.829 \pm 0.012 \qquad (Planck + \mathrm{WP}), \tag{16}$$

$$\sigma_8 = 0.814 \pm 0.014 \qquad (Planck\text{-}A_L + \mathrm{WP}). \tag{17}$$

These shifts bring *Planck* in much better agreement with *WMAP*9. Since we still have a high value of σ_8 compared to the growth of structure measurements, we still have a preference for a neutrino mass, similar to the results in *WMAP*9.

Combining *Planck* $- A_L$ with the results of Beutler et al. (2014) produces $\sum m_\nu = 0.34 \pm 0.14$ eV, in excellent agreement with the result obtained when combining with *WMAP*9. Including CFHTLenS yields $\sum m_\nu = 0.38 \pm 0.11$ eV, and adding galaxy–galaxy lensing and further BAO constraints improves this detection to $\sum m_\nu = 0.36 \pm 0.10$ eV (3.4σ). This detection is robust against various data set variations as shown in Table 2. The results are also presented in Figs 7 (lower two plots) and 8 (middle).

5.4 Combining with the *Planck* re-analysis of Spergel et al. (2013)

Spergel et al. (2013) re-analysed the *Planck* data with a different treatment for foreground cleaning, which has a notable effect

[4] http://irsa.ipac.caltech.edu/data/Planck/release_1/ancillary-data/

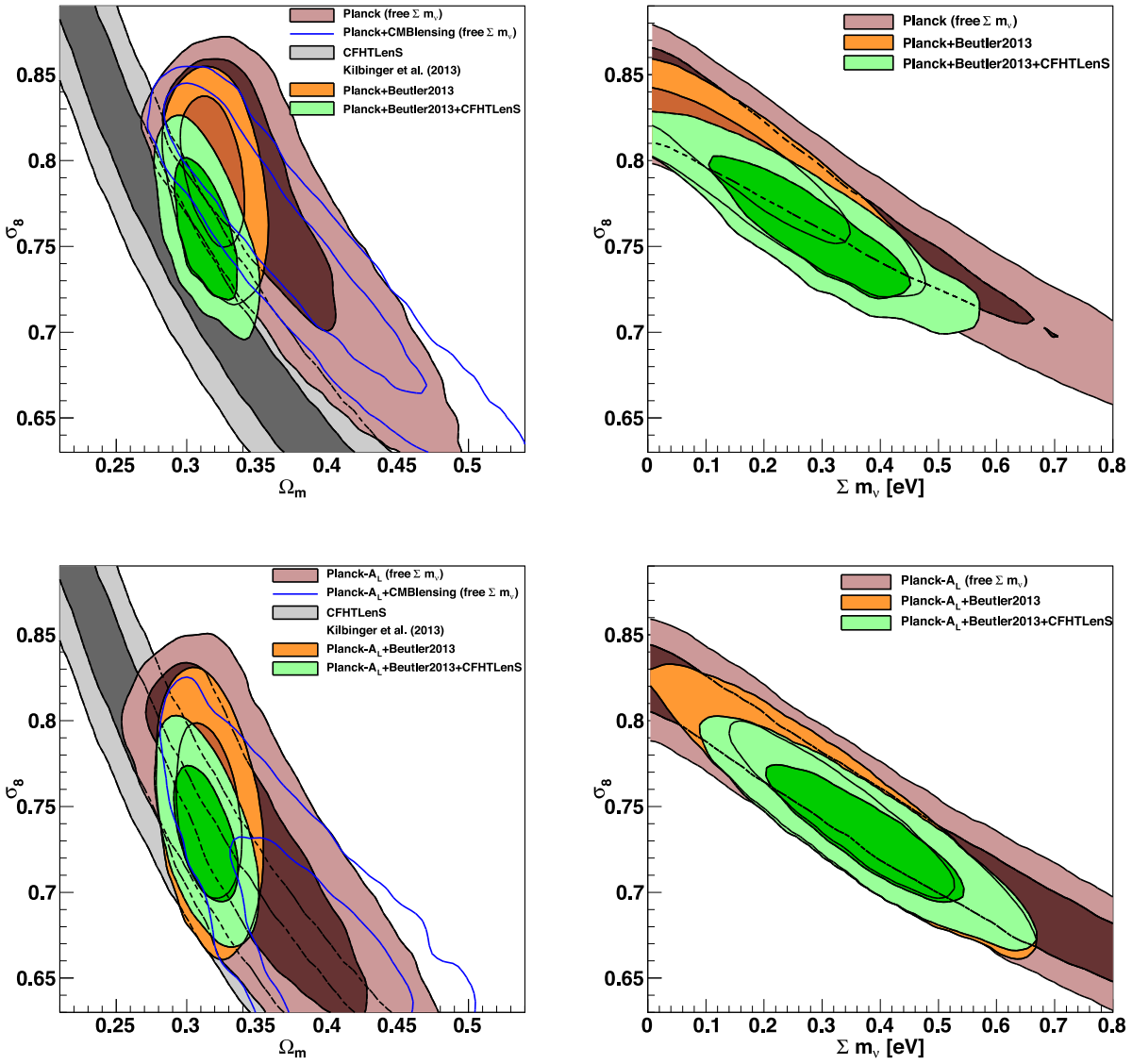

Figure 7. Two-dimensional likelihood for $\Omega_{\rm m}$–σ_8 (left) and $\sum m_\nu$–σ_8 (right) when combining *Planck* MCMC chains within ΛCDM and free $\sum m_\nu$ with different low-redshift growth of structure constraints. We show the main *Planck* results in the two plots on the top. The two bottom plots show the results where we used a *Planck* MCMC chain with the $A_{\rm L}$ lensing signal marginalized out. The orange contours show *Planck* combined with the $D_{\rm V}/r_{\rm s}$, $F_{\rm AP}$ and $f\sigma_8$ constraints of Beutler et al. (2014). The green contours additionally include CFHTLenS. The blue contours show *Planck* and *Planck*–$A_{\rm L}$ combined with CMB lensing from the four-point function (top left and bottom left, respectively). The results are summarized in Table 2.

on the 217 GHz spectra. From now on we will call this analysis Spergel2013. Their result show $\sim 1\sigma$ shifts in σ_8 and $\Omega_{\rm m}$ towards smaller values. Similar shifts caused by different foreground removal techniques have been reported by the *Planck* collaboration (Planck Collaboration XII 2013a). These changes in $\Omega_{\rm m}$ and σ_8 are smaller, but similar to the shifts we found by excluding the $A_{\rm L}$ lensing contribution. We saw that such shifts can significantly alter the constraints on $\sum m_\nu$.

We now use the MCMC chains of Spergel et al. (2013), where the neutrino mass is varied freely and importance sample these chains. The chains we use include the $A_{\rm L}$ lensing signal, meaning they do not marginalize over $A_{\rm L}$. The CMB lensing signal from the four-point function is not included. The result is shown in Figs 8 (bottom) and 9 and Table 2. Combining Spergel2013 with the results of Beutler et al. (2014) yields $\sum m_\nu = 0.24 \pm 0.12$ eV. Including CFHTLenS, GGlensing and further BAO constraints gives $\sum m_\nu = 0.29 \pm 0.10$ eV (2.9σ). These results are within 1σ with the results we obtained when importance sampling the *Planck* and the *Planck*–$A_{\rm L}$ chains. Overall we see small (below 1σ) shifts towards *WMAP*.

6 DISCUSSION

We can summarize the results of the last section as follows.

(i) We have a significant ($>3\sigma$) detection of the neutrino mass when combining *WMAP*9 and *Planck* $-$ $A_{\rm L}$ with low-redshift growth of structure constraints. *Planck* $-$ $A_{\rm L}$ represents the *Planck* data set without the lensing contribution to the temperature power spectrum.

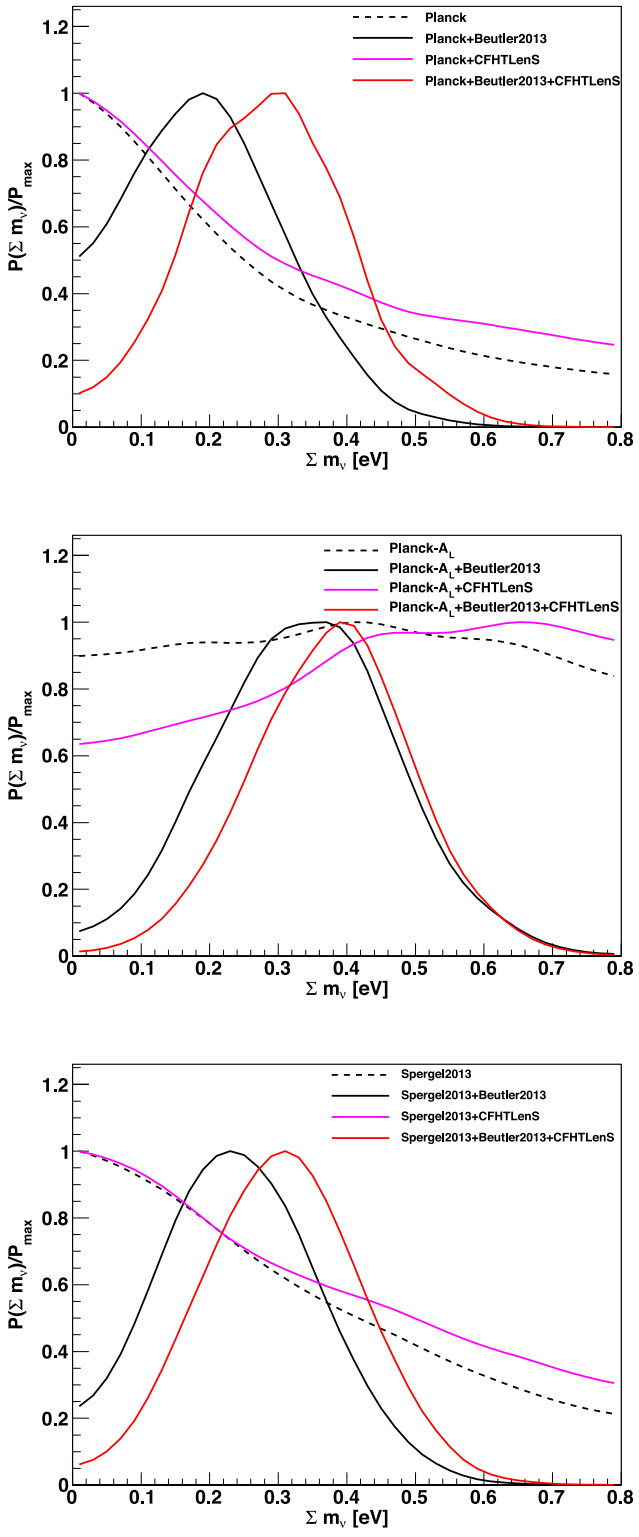

Figure 8. One-dimensional likelihood distribution for $\sum m_\nu$ when combining *Planck* with different data sets. We show the results for the main *Planck* data set (top), the *Planck* data set without the $A_{\rm L}$ lensing signal (middle) and the *Planck* re-analysis of Spergel et al. (2013) (bottom). Beutler2013 stands for the $D_{\rm V}/r_{\rm s}$, $F_{\rm AP}$ and $f\sigma_8$ constraints of Beutler et al. (2014), while CFHTLenS represents the constraint reported in Kilbinger et al. (2013).

(ii) The $A_{\rm L}$ lensing contribution leads to $\sim 1\sigma$ shifts in $\Omega_{\rm m}$ and σ_8, which have a non-negligible impact on the neutrino mass constraints.

(iii) When using *Planck* including the lensing contribution to the temperature power spectrum the significance of the detection of the neutrino mass is reduced to $\sim 2\sigma$.

(iv) The *Planck* re-analysis by Spergel et al. (2013) shows results very similar to *Planck* with a slightly increased significance for the neutrino mass.

It might not be too surprising that excluding the $A_{\rm L}$ lensing result brings *Planck* closer to *WMAP*9, since the $A_{\rm L}$ lensing contribution is unique to *Planck* and removing it increases the fraction of information common to the two data sets. Nevertheless, since there is a 2σ tension between the $A_{\rm L}$ lensing and the CMB lensing in the four-point function, it is interesting to examine the *Planck* data excluding the $A_{\rm L}$ lensing signal, especially given the shifts in σ_8 and $\Omega_{\rm m}$, which significantly alter the constraints on $\sum m_\nu$.

The left-hand panels in Figs 5, 7 and 9 show how the two-dimensional constraints on $\Omega_{\rm m}$ and σ_8 migrate when different data sets are included. The external data sets pull the combined constraint out of the 68 per cent confidence region of *Planck* (top panel of Fig. 7), indicating that increasing $\sum m_\nu$ does not resolve the tension between *Planck* and low-redshift growth of structure constraints. *WMAP*9 and *Planck* $- A_{\rm L}$ present a different situation. Here the final constraints using all data sets lie within the 68 per cent confidence region of the CMB data sets.

Figs 6 and 8 display the one-dimensional likelihood of $\sum m_\nu$ when combining low-redshift growth of structure data sets with *WMAP*9, *Planck*, *Planck* $- A_{\rm L}$ and Spergel2013. While there is a prominent detection in the case of *WMAP*9 and *Planck* $- A_{\rm L}$, the detection in *Planck* is of low significance. The *Planck* re-analysis of Spergel et al. (2013) shows a likelihood distribution very similar to the one obtained with the main *Planck* analysis.

We also note that there is tension between different components of the *Planck* data set. While the amplitude of the $A_{\rm L}$ lensing in the two-point function prefers a small neutrino mass, the shape of the CMB lensing in the four-point function prefers a large neutrino mass. In Table 2 we can see that after marginalizing over $A_{\rm L}$ the *Planck* data set combined with CMB lensing prefers a neutrino mass of 0.86 eV with more than 2σ.

To quantify the differences between the *Planck* and *Planck* $- A_{\rm L}$ chains used in this analysis we can look at $\Delta\chi^2$ for the best-fitting cosmological parameters when combining the CMB data sets with Beutler et al. (2014), CFHTLenS, galaxy–galaxy lensing and the BAO constraints of 6dFGS and LOWZ. Within ΛCDM we find $\chi^2_{\rm Planck} - \chi^2_{{\rm Planck}-A_{\rm L}} = 9.5$, while for ΛCDM+$\sum m_\nu$ we have $\Delta\chi^2 = 14.5$. In both cases the χ^2 is reduced when excluding the $A_{\rm L}$ lensing contribution. We can also quantify which data sets drive the preference for neutrino mass. Considering the following data set combinations (*Planck*, *Planck*+BAO, CFHTLenS+GGlensing, Beutler2013, Beutler2013$_{\rm BAOonly}$), where BAO stands for the BAO constraints of 6dFGS and LOWZ, Beutler2013 stands for the three CMASS constraints ($D_{\rm V}/r_{\rm s}$, $F_{\rm AP}$, $f\sigma_8$) of Beutler et al. (2014) and Beutler2013$_{\rm BAOonly}$ represents only the BAO constraint ($D_{\rm V}/r_{\rm s}$). Note that $F_{\rm AP}$ and $f\sigma_8$ of Beutler et al. (2014) are correlated and we cannot easily explore the effect of just one of these constraints. We find the following $\Delta\chi^2$ values for the best-fitting cosmology, when comparing ΛCDM and ΛCDM+$\sum m_\nu$: (−4.3, −4.0, 2.8, 4.1, 0.3). The preference for neutrino mass in the case of *Planck* is driven by the CMASS and lensing constraints. If we instead use the best-fitting

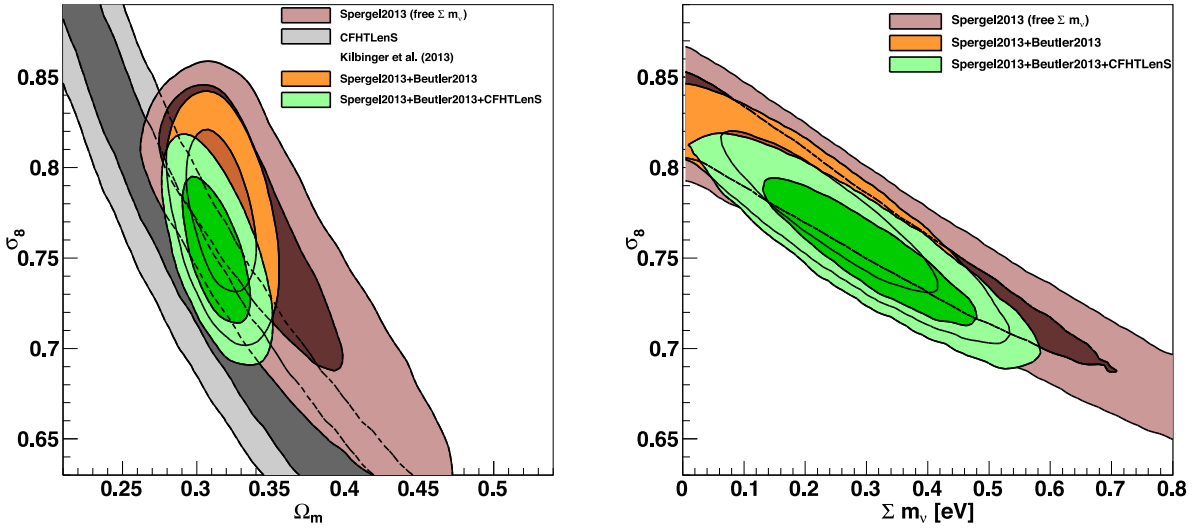

Figure 9. Two-dimensional likelihood for Ω_m–σ_8 (left) and $\sum m_\nu$–σ_8 (right) when combining the *Planck* re-analysis of Spergel et al. (2013) within ΛCDM and free $\sum m_\nu$ with different low-redshift growth of structure constraints. The orange contours show the *Planck* re-analysis combined with the D_V/r_s, F_{AP} and $f\sigma_8$ constraints of Beutler et al. (2014). The green contours additionally include CFHTLenS. The results are summarized in Table 2.

cosmological parameters in the case of *Planck* $-A_L$ and again consider the data set combinations (*Planck* $-A_L$, *Planck* $-A_L$+BAO, CFHTLenS+GGlensing, Beutler2013, Beutler2013$_{BAOonly}$) we find $\Delta\chi^2 = (0.7, -0.17, 3.9, 4.8, 0.5)$. Again the preference for neutrino mass is driven by the CMASS and lensing constraints. Comparing Beutler2013 and Beutler2013$_{BAOonly}$ we see that it is mainly the RSD (and AP) constraints which drive the preference for neutrino mass within CMASS.

While in this paper we focus on the neutrino mass as a possible extension to ΛCDM, it is interesting to ask whether other parameters would also be able to alleviate the tension between the different data sets discussed in this paper. Comparing the best-fitting χ^2 of a universe with curvature as a free parameter (oCDM) to the best-fitting χ^2 when varying the neutrino mass we find $\Delta\chi^2 = \chi^2_{oCDM} - \chi^2_{\sum m_\nu \Lambda CDM} = 6.27$, meaning that the neutrino mass is preferred as an extension to ΛCDM. Including instead a dark energy equation of state parameter (wCDM) we find $\Delta\chi^2 = \chi^2_{wCDM} - \chi^2_{\sum m_\nu \Lambda CDM} = 0.68$, showing only mild preference for the neutrino mass parameter. If we include the neutrino mass as well as the number of relativistic species, N_ν, as free parameters we find $\Delta\chi^2 = \chi^2_{N_\nu \sum m_\nu \Lambda CDM} - \chi^2_{\sum m_\nu \Lambda CDM} = -0.99$. While the χ^2 is reduced, the reduction of χ^2 is not sufficient to justify the new parameter. We also note that the new parameter N_ν does not remove the preference for a non-zero neutrino mass, with the best-fitting values being $N_\nu = 3.61 \pm 0.35$ and $\sum m_\nu = 0.46 \pm 0.18$.

Combining CMB data sets with external information on the Hubble parameter allows one to break the geometric degeneracy between H_0 and the neutrino mass parameter (Komatsu et al. 2009) similar to the BAO constraints. A large neutrino mass leads to a smaller Hubble Constant and vice versa. Since the low-redshift H_0 constraints using the distance ladder technique seem to find large values of H_0 (Riess et al. 2011; Freedman et al. 2012; Efstathiou 2014) compared to CMB or BAO measurements, including the low-redshift H_0 constraints usually does not lead to a detection of the neutrino mass (see e.g. Hou et al. 2014; Riemer-Sorensen et al. 2014; Verde, Protopapas & Jimenez 2013; de Putter, Linder & Mishra 2014; Zheng et al. 2014).

Sanchez et al. (2014) reported an upper limit on the neutrino mass of $\sum m_\nu < 0.23$ eV (95 per cent c.l.) using data from *Planck*, ACT and SPT, combined with CMASS-DR11. Their use of the CMASS-DR11 data set is different to our analysis, since they make use of the shape of the correlation function wedges. Nevertheless, their result is consistent with our 95 per cent confidence level upper limit in *Planck*. When using *WMAP*9 instead of *Planck*, Sanchez et al. (2014) find $\sum m_\nu = 0.23 \pm 0.12$ eV, which again is in 1σ agreement with our result.

A tight constraint on the neutrino mass of $\sum m_\nu < 0.17$ eV (95 per cent c.l.) has been reported in Seljak et al. (2006) by combining Lyα forest power spectrum information with *WMAP*3 as well as supernovae and galaxy clustering constraints. One reason they achieved such a tight constraint was that their Lyα forest measurement was in tension with *WMAP*3. Since this Lyα forest measurement is now in good agreement with *Planck*, their upper limit would weaken.

In addition to these non-detections, there are many studies which report a detection of the neutrino mass (see e.g. Hou et al. 2014; Planck Collaboration XX 2013e; Rozo et al. 2013; Wyman et al. 2014). Battye & Moss (2014) showed that the *Planck*+CFHTLenS constraints are compatible with the constraints obtained when combining *Planck* with the SZ cluster results also reported by the *Planck* team. They then performed an analysis combining *Planck* with BAO, CFHTLenS and SZ clusters finding $\sum m_\nu = 0.320 \pm 0.081$ eV, which is in good agreement with our results. This constraint is however dominated by the SZ cluster constraint which suffers from various systematic errors (Rozo et al. 2014, 2013; Costanzi et al. 2013; Paranjape 2014; von der Linden et al. 2014).

6.1 Implications for general relativity

Beutler et al. (2014) combined CMASS-DR11 results with *Planck* and *WMAP*9 to test general relativity (GR) using the simple γ-parametrization, where the growth rate is given by $f(z) \simeq \Omega_m^\gamma(z)$ (Linder 2005). Beutler et al. (2014) found $\gamma = 0.772^{+0.124}_{-0.097}$ when combining with *Planck* and $\gamma = 0.76 \pm 0.11$ when combining with *WMAP*9. These results are in 2σ tension with the GR prediction of

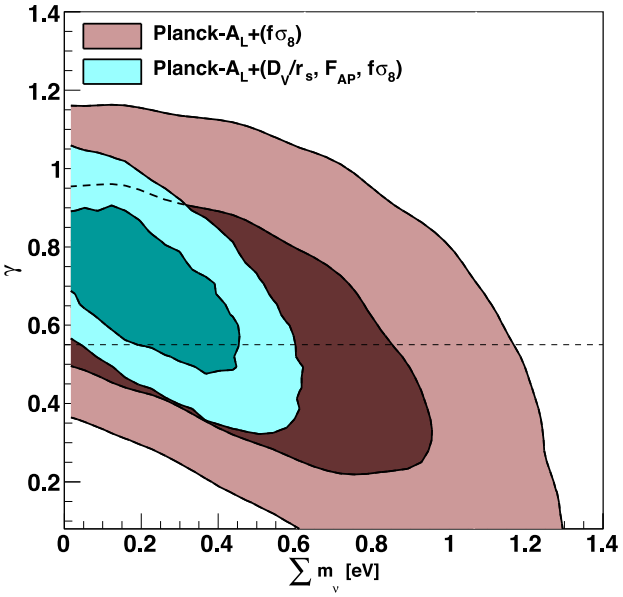

Figure 10. Two-dimensional likelihood of the growth index γ and $\sum m_\nu$. We combine different parts of the CMASS results of Beutler et al. (2014) with *Planck* $-$ $A_{\rm L}$. *Planck* $-$ $A_{\rm L}$ is the *Planck* data set where the $A_{\rm L}$ lensing contribution has been marginalized out. Combining *Planck* $-$ $A_{\rm L}$ with the $D_{\rm V}/r_{\rm s}$, $F_{\rm AP}$ and $f\sigma_8$ constraint of Beutler et al. (2014) (cyan contours) produces constraints on γ in good agreement with the prediction by GR (black dashed line).

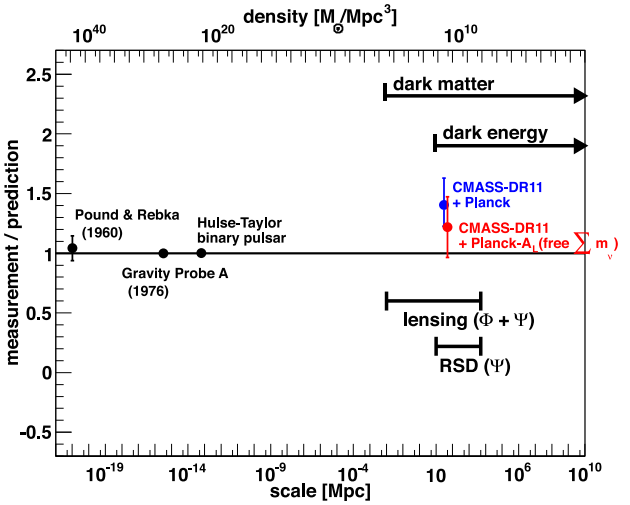

Figure 11. Summary of different tests of GR as a function of distance scale (bottom axis) and densities (top axis). The figure includes the Pound–Rebka experiment (Pound & Rebka 1960), Gravity Probe A (Vessot et al. 1980) and the Hulse–Taylor binary pulsar (Hulse & Taylor 1975). The error bars for Gravity Probe A and the Hulse–Taylor binary pulsar are smaller than the data points in this plot. In blue we include the result of Beutler et al. (2014), where *Planck* (within ΛCDM) has been combined with CMASS-DR11 constraints, finding a 2σ tension. In this analysis we use the *Planck* result where the $A_{\rm L}$ lensing contribution has been marginalized out and vary $\sum m_\nu$ (red data point).

$\gamma^{\rm GR} \approx 0.55$. The question is now, what are the implications of a neutrino mass for these results?

As discussed in Beutler et al. (2014), the tension with GR is mainly caused by the large σ_8 in the CMB data sets. Since introducing a neutrino mass reduces the CMB prediction of σ_8, we can expect that a non-zero neutrino mass will also decrease the tension with GR. The reason to combine the clustering result of CMASS with a CMB data set is the need to add information on σ_8 to be able to test gravity through the growth rate $f(z)$. Since the uncertainty in σ_8 significantly increases when the neutrino mass is varied freely, we expect that the error on γ will increase as well.

Here we use the two CMB chains with the strongest signs of a neutrino mass, which are *WMAP*9 and *Planck* $-$ $A_{\rm L}$. We use the chains which have the sum of the neutrino masses as a free parameter. We importance sample these chains and include γ as an additional free parameter following the procedure of section 9.1 in Beutler et al. (2014). Marginalizing over all other parameters we find $\gamma = 0.72 \pm 0.19$ for *WMAP*9 and $\gamma = 0.67 \pm 0.14$ for *Planck* $-$ $A_{\rm L}$. Both results are in 1σ agreement with the GR prediction. The result for the *Planck* $-$ $A_{\rm L}$ chain is shown in Figs 10 and 11. Even though the constraints on the sum of the neutrino masses for this test are significantly degraded, because of the degeneracy with γ, we include them in Table 3. Fig. 11 compares the result of this analysis (red data point) with the result in Beutler et al. (2014) (blue data point). It might not be surprising that the tension with GR in Beutler et al. (2014) can be reduced by introducing a new parameter, especially if this parameter is degenerate with γ.

6.2 Implications for particle physics

Although our evidence of the neutrino mass has to be taken with care given the significance of the detection ($\sim$2.5–3.5σ) and the tension with the $A_{\rm L}$ lensing contribution to the *Planck* measurement, it is still interesting to investigate the implications of such a result.

What are the implications for the masses of the neutrino eigenstates? We use the mass difference $|\Delta m^2_{31}| = 2.4 \times 10^{-3}$ eV^2 (Beringer et al. 2012) and our measurement $\sum m_\nu = 0.36 \pm 0.10$ eV, which was obtained by combining *Planck* $-$ $A_{\rm L}$ with Beutler et al. (2014), CFHTLenS, galaxy–galaxy lensing and BAO constraints from 6dFGS and LOWZ. If we further assume three neutrinos arranged by the normal hierarchy with the two light neutrinos ($m_{\nu_{1,2}}$) having the same mass, we find $m_{\nu_3} = 0.127 \pm 0.032$ eV and $m_{\nu_{1,2}} = 0.117 \pm 0.032$ eV. For the inverted hierarchy we get instead $m_{\nu_{1,2}} = 0.123 \pm 0.032$ eV and $m_{\nu_3} = 0.113 \pm 0.032$ eV.

Given a certain hierarchy we can calculate the flavour eigenstates using the mixing matrix (Pontecorvo–Maki–Nakagawa–Sakata matrix):

$$U_{\rm PMNS} = \begin{pmatrix} 0.82 & 0.55 & 0.15 \\ -0.50 & 0.58 & 0.64 \\ 0.26 & -0.60 & 0.75 \end{pmatrix}, \quad (18)$$

where we assume any possible complex phase to be zero and use the mixing angles from Beringer et al. (2012) and An et al. (2013). The flavour eigenstates are then given as superposition of the mass eigenstates:

$$\begin{pmatrix} |\nu_e\rangle \\ |\nu_\mu\rangle \\ |\nu_\tau\rangle \end{pmatrix} = U_{\rm PMNS} \begin{pmatrix} |\nu_1\rangle \\ |\nu_2\rangle \\ |\nu_3\rangle \end{pmatrix}. \quad (19)$$

Because of neutrino mixing, the observable of different direct neutrino mass experiments is different to the flavour states. Neutrinoless double β-decay ($0\nu\beta\beta$) experiments are sensitive to the mass:

$$m_{\beta\beta} = \sum_{i=1}^{3} m_{\nu_i} U^2_{\rm PMNS,1i}, \quad (20)$$

Table 3. Constraints on the growth index γ and the sum of the neutrino masses from *WMAP*9 and *Planck* $-A_{\rm L}$ combined with the constraints of Beutler et al. (2014). For γ we show 1σ errors, while for the sum of the neutrino masses we report the 68 and 95 per cent confidence levels. The constraints on $\sum m_\nu$ are significantly degraded compared to the results in Table 2 because of the degeneracy with γ. The last two rows show the constrains obtained in Beutler et al. (2014) within ΛCDM for comparison.

Data set(s)	γ	$\sum m_\nu$ (eV)	
		68 per cent c.l.	95 per cent c.l.
*WMAP*9+Beutler2013	0.72 ± 0.19	$0.47^{+0.23}_{-0.32}$	<0.85
Planck $-A_{\rm L}$+Beutler2013	0.67 ± 0.14	$0.25^{+0.13}_{-0.22}$	<0.52
*WMAP*9+Beutler2013 (ΛCDM)	0.76 ± 0.11	–	–
Planck+Beutler2013 (ΛCDM)	$0.772^{+0.124}_{-0.097}$	–	–

while β-decay experiments are sensitive to

$$m_\beta = \sqrt{\sum_{i=1}^{3} m_{\nu_i}^2 U_{\rm PMNS,1i}^2}. \quad (21)$$

Taking the constraints on the mass eigenstates above together with the mixing matrix we find $m_\beta = 0.117 \pm 0.031$ eV for the normal hierarchy and $m_\beta = 0.123 \pm 0.032$ eV for the inverted hierarchy.[5] Since the masses are close to degenerate and because $U_{\rm PMNS,13}$ is small compared to $U_{\rm PMNS,11}$ and $U_{\rm PMNS,12}$, the values of m_β are basically identical to $m_{\nu_{1,2}}$. The value of m_β in both hierarchies is below the predicted sensitivity range of the KATRIN experiment.

7 CONCLUSION

This paper presents an investigation of the cosmological implications of the CMASS-DR11 anisotropic analysis including the growth of structure measurement, with particular focus on the sum of the neutrino masses $\sum m_\nu$.

First we examine the robustness of the CMASS constraints of Beutler et al. (2014) when changing the power spectrum template including $\sum m_\nu = 0.4$ eV. Our main cosmological parameters change by $<0.5\sigma$ and therefore are robust against variations in the neutrino mass. We perform similar tests for the weak lensing results from CFHTLenS, finding that these results show only weak dependence on the initial assumption of the neutrino mass parameter.

We use the *WMAP*9 and *Planck* MCMC chains where the sum of the neutrino masses is varied as a free parameter and importance sample these chains. When combining *WMAP*9 with the three constraints ($D_{\rm V}/r_{\rm s}$, $F_{\rm AP}$, $f\sigma_8$) of Beutler et al. (2014) we obtain $\sum m_\nu = 0.36 \pm 0.14$ eV, which represents a 2.6σ preference for the neutrino mass. If we also include CFHTLenS, galaxy–galaxy lensing and the BAO constraints from 6dFGS and LOWZ, we find $\sum m_\nu = 0.35 \pm 0.10$ eV (3.3σ).

Using the *Planck* data set the preference for a neutrino mass is reduced to $\sim 2\sigma$. However, marginalizing over the $A_{\rm L}$ lensing contribution to the temperature power spectrum of *Planck* leads to $\sim 1\sigma$ shifts in $\Omega_{\rm m}$ and σ_8, which bring *Planck* into much better agreement with *WMAP*9. Combining *Planck* without the $A_{\rm L}$ lensing contribution with CMASS yields similar results to *WMAP*9. We find $\sum m_\nu = 0.36 \pm 0.10$ eV (3.4σ) when combining with Beutler et al. (2014), CFHTLenS, galaxy–galaxy lensing and further BAO constraints. This constraint is robust against various permutations of data sets (see Table 2 for details). We also investigated the *Planck* re-analysis of Spergel et al. (2013), finding that it yields results very similar to *Planck* with a slightly increased significance for a neutrino mass. While the preference for neutrino mass is driven mainly by the low-redshift growth of structure constraints it is reassuring that the three growth of structure data sets included in this analysis (CMASS-RSD, CFHTLenS and galaxy–galaxy lensing) yield consistent results. Our constraints could be significantly improved by including cluster counts detected through the SZ effect. We chose, however, to not include these data sets, because of the significant systematic uncertainty of these measurements with respect to the treatment of the neutrino mass.

In this paper we present many combinations of data sets and a natural question is, which of these presents the main result of this paper. When discussing the implications of our results in Section 6.2, we selected the constraint $\sum m_\nu = 0.35 \pm 0.10$ eV, obtained with the *Planck* $-A_{\rm L}$ chain. However, we cannot conclusively put this forward as the fiducial result of our analysis, without having an explanation for the tension with the $A_{\rm L}$ lensing amplitude. The origin of the tension between the different components in the *Planck* data set remains an open question, which we will hopefully learn more about with the next data release of *Planck*.

A neutrino mass at this level would relieve the tension of current data sets with the clustering prediction of GR reported in Beutler et al. (2014). If we remove the $A_{\rm L}$ lensing contribution to *Planck* and combine with the ($D_{\rm V}/r_{\rm s}$, $F_{\rm AP}$, $f\sigma_8$) constraints of Beutler et al. (2014) by varying the neutrino mass and the growth index γ as free parameters, where $f(z) = \Omega_{\rm m}^\gamma(z)$, we find $\gamma = 0.67 \pm 0.14$. This result is in 1σ agreement with the GR prediction of $\gamma^{\rm GR} = 0.55$. Similar results are obtained for *WMAP*9.

If our result is confirmed by future, more precise cosmological measurements, it will have significant implications for particle physics and cosmology. The constraint $\sum m_\nu = 0.35 \pm 0.10$ eV can be expressed as

$$\Omega_\nu h^2 = 0.0039 \pm 0.0011 \quad \text{or} \quad (22)$$

$$f_\nu = 0.0315 \pm 0.0088. \quad (23)$$

The large value of $\sum m_\nu$ found in our analysis would be too large to allow for cosmological probes to distinguish between the inverted and the normal mass hierarchies just by the measurement of the sum of the masses. However, within the normal hierarchy we can predict $m_\beta = 0.117 \pm 0.031$ eV, while for the inverted hierarchy we find $m_\beta = 0.123 \pm 0.032$ eV. These masses are below the predicted detection limits of the KATRIN experiment (assuming a sensitivity of $m_\beta \sim 0.2$ eV; Wolf 2010).

[5] The errors on the mixing angles are not propagated, since the error budget is dominated by the uncertainty in the sum of the neutrino masses.

The constraints presented in this paper will be further improved in the near future. Within the CMASS data set the weakest point of the constraint is certainly the large uncertainty on $f\sigma_8$, which, however, is predicted to improve significantly with future data sets like the Dark Energy Spectroscopic Instrument (DESI; Abazajian et al. 2013; Font-Ribera et al. 2014). Even the BOSS data set could provide additional constraints on the neutrino mass using the characteristic scale-dependent damping of the power spectrum (see Zhao et al. 2013 for such an attempt) which, however, requires refined simulations including massive neutrinos (Villaescusa-Navarro et al. 2014).

ACKNOWLEDGEMENTS

We would like to thank Renee Hlozek for providing the MCMC chains for the *Planck* re-analysis. FB would like to thank Martin Kilbinger and Catherine Heymans for help with the CFHTLenS data set and CosmoPMC. FB would also like to thank Martin White, Uros Seljak, Eric Linder, Daniel Dwyer, Morag Scrimgeour, Michael Mortonson, Marcel Schmittful and Blake Sherwin for helpful discussion. SS would like to thank Kiyotomo Ichiki and Masahiro Takada for providing their MCMC code for weak lensing analysis and for useful discussions. SS is supported by a Grant-in-Aid for Young Scientists (Start-up) from the Japan Society for the Promotion of Science (JSPS) (No. 25887012).

Funding for SDSS-III has been provided by the Alfred P. Sloan Foundation, the Participating Institutions, the National Science Foundation and the US Department of Energy Office of Science. The SDSS-III web site is http://www.sdss3.org/.

SDSS-III is managed by the Astrophysical Research Consortium for the Participating Institutions of the SDSS-III Collaboration including the University of Arizona, the Brazilian Participation Group, Brookhaven National Laboratory, Carnegie Mellon University, University of Florida, the French Participation Group, the German Participation Group, Harvard University, the Instituto de Astrofisica de Canarias, the Michigan State/Notre Dame/JINA Participation Group, Johns Hopkins University, Lawrence Berkeley National Laboratory, Max Planck Institute for Astrophysics, Max Planck Institute for Extraterrestrial Physics, New Mexico State University, New York University, Ohio State University, Pennsylvania State University, University of Portsmouth, Princeton University, the Spanish Participation Group, University of Tokyo, University of Utah, Vanderbilt University, University of Virginia, University of Washington and Yale University.

This research used resources of the National Energy Research Scientific Computing Center, which is supported by the Office of Science of the US Department of Energy under Contract No. DE-AC02-05CH11231.

REFERENCES

Abazajian K. N. et al. [SDSS Collaboration], 2009, ApJS, 182, 543
Abazajian K. N. et al., 2013, Astropart. Phys., preprint (arXiv:1309.5383)
Ahn C. P. et al. [SDSS Collaboration], 2012, ApJS, 203, 21
An F. P. et al. [Daya Bay Collaboration], 2013, Phys. Rev. Lett., preprint (arXiv:1310.6732)
Anderson L. et al., 2014a, MNRAS, 439, 83
Anderson L. et al., 2014b, MNRAS, 441, 24
Battye R. A., Moss A., 2014, Phys. Rev. Lett., 112, 051303
Benjamin J. et al., 2013, MNRAS, 431, 1547
Benson B. A. et al., 2013, ApJ, 763, 147
Beringer J. et al. [Particle Data Group Collaboration], 2012, Phys. Rev. D, 86, 010001
Beutler F. et al., 2011, MNRAS, 416, 3017
Beutler F. et al., 2012, MNRAS, 423, 3430
Beutler F. et al., 2014, MNRAS, 443, 1065
Bird S., Viel M., Haehnelt M. G., 2012, MNRAS, 420, 2551
Blake C. et al., 2011, MNRAS, 415, 2876
Bolton A. S. et al. [Cutler Group LP Collaboration], 2012, AJ, 144, 144
Bond J. R., Efstathiou G., Silk J., 1980, Phys. Rev. Lett., 45, 1980
Brandbyge J., Hannestad S., Haugbolle T., Thomsen B., 2008, J. Cosmol. Astropart. Phys., 08, 020
Burenin R. A., 2013, Astron. Lett., 39, 357
Chuang C.-H. et al., 2013, preprint (arXiv:1312.4889)
Costanzi M., Villaescusa-Navarro F., Viel M., Xia J.-Q., Borgani S., Castorina E., Sefusatti E., 2013, J. Cosmol. Astropart. Phys., 12, 012
Das S. et al., 2014, J. Cosmol. Astropart. Phys., 04, 014
Dawson K. S. et al. [BOSS Collaboration], 2013, AJ, 145, 10
de Putter R. et al., 2012, ApJ, 761, 12
de Putter R., Linder E. V., Mishra A., 2014, Phys. Rev. D, 89, 103502
Dodelson D., Gates E., Stebbins A., 1996, ApJ, 467, 10
Doi M. et al., 2010, AJ, 139, 1628
Dunkley J. et al. [WMAP Collaboration], 2009, ApJS, 180, 306
Efstathiou G., 2014, MNRAS, 440, 1138
Eisenstein D. J., Hu W., 1998, ApJ, 496, 605
Eisenstein D. J., Hu W., 1999, ApJ, 511, 5
Eisenstein D. J. et al. [SDSS Collaboration], 2011, AJ, 142, 72
Erben T. et al., 2013, MNRAS, 433, 2545
Font-Ribera A., McDonald P., Mostek N., Reid B. A., Seo H.-J., Slosar A., 2014, J. Cosmol. Astropart. Phys., 05, 023
Freedman W. L., Madore B. F., Scowcroft V., Burns C., Monson A., Persson S. E., Seibert M., Rigby J., 2012, ApJ, 758, 24
Fukugita M., Ichikawa T., Gunn J. E., Doi M., Shimasaku K., Schneider D. P., 1996, AJ, 111, 1748
Gando A. et al. [KamLAND-Zen Collaboration], 2013, Phys. Rev. Lett., 110, 062502
Giusarma E., de Putter R., Ho S., Mena O., 2013, Phys. Rev. D, 88, 063515
Gong Y., Zhang T.-J., Lan T., Chen X.-L., 2008, preprint (arXiv:0810.3572)
Gunn J. E. et al. [SDSS Collaboration], 1998, AJ, 116, 3040
Gunn J. E. et al. [SDSS Collaboration], 2006, AJ, 131, 2332
Hamann J., Hasenkamp J., 2013, J. Cosmol. Astropart. Phys., 10, 044
Hawkins E. et al., 2003, MNRAS, 346, 78
Heymans C. et al., 2012, MNRAS, 427, 146
Hildebrandt H. et al., 2012, MNRAS, 421, 2355
Hinshaw G. et al. [WMAP Collaboration], 2009, ApJS, 180, 225
Hinshaw G. et al. [WMAP Collaboration], 2013, ApJS, 208, 19
Hou Z. et al., 2014, ApJ, 782, 74
Hu W., Eisenstein D. J., Tegmark M., 1998, Phys. Rev. Lett., 80, 5255
Hulse R. A., Taylor J. H., 1975, ApJ, 195, L51
Ichikawa K., Fukugita M., Kawasaki M., 2005, Phys. Rev. D, 71, 043001
Ichiki K., Takada M., Takahashi T., 2009, Phys. Rev. D, 79, 023520
Keisler R. et al., 2011, ApJ, 743, 28
Kilbinger M., Benabed K., Cappe O., Cardoso J.-F., Fort G., Prunet S., Robert C. P., Wraith D., 2011, preprint (arXiv:1101.0950)
Kilbinger M. et al., 2013, MNRAS, 430, 2200
Komatsu E. et al. [WMAP Collaboration], 2009, ApJS, 180, 330
Komatsu E. et al. [WMAP Collaboration], 2011, ApJS, 192, 18
Lesgourgues J., Pastor S., 2006, Phys. Rep., 429, 307
Lesgourgues J., Pastor S., 2012, Adv. High Energy Phys., 2012, 608515
Lesgourgues J., Mangano G., Miele G., Pastor S., 2013, Neutrino Cosmology. Cambridge Univ. Press, Cambridge
Lewis A., Bridle S., 2002, Phys. Rev. D, 66, 103511
Li H., Liu J., Xia J.-Q., Sun L., Fan Z.-H., Tao C., Tilquin A., Zhang X., 2009, Phys. Lett. B, 675, 164
Linder E. V., 2005, Phys. Rev. D, 72, 043529
Lobashev V. M. et al., 1999, Phys. Lett. B, 460, 227
Mandelbaum R., Slosar A., Baldauf T., Seljak U., Hirata C. M., Nakajima R., Reyes R., Smith R. E., 2013, MNRAS, 432, 1544
Miller L. et al., 2013, MNRAS, 429, 2858
Oka A., Saito S., Nishimichi T., Taruya A., Yamamoto K., 2014, MNRAS, 439, 2515

Paranjape A., 2014, Phys. Rev. D, 90, 023520
Planck Collaboration XII, 2013a, A&A, submitted (arXiv:1303.5072)
Planck Collaboration XVI, 2013b, preprint (arXiv:1303.5076)
Planck Collaboration XVIII, 2013c, A&A, submitted (arXiv:1303.5078)
Planck Collaboration XIX, 2013d, preprint (arXiv:1303.5079)
Planck Collaboration XX, 2013e, A&A, preprint (arXiv:1303.5080)
Pound R. V., Rebka G. A., Jr, 1960, Phys. Rev. Lett., 4, 337
Reid B. A., Verde L., Jimenez R., Mena O., 2010, J. Cosmol. Astropart. Phys., 01, 003
Riemer-Sorensen S., Parkinson D., Davis T. M., 2014, Phys. Rev. D, 89, 103505
Riess A. G. et al., 2011, ApJ, 730, 119 [Erratum-ibid. 732, 129 (2011)]
Ross A. J. et al., 2014, MNRAS, 437, 1109
Rozo E., Rykoff E. S., Bartlett J. G., Evrard A. E., 2013, preprint (arXiv:1302.5086)
Rozo E., Rykoff E. S., Bartlett J. G., Evrard A. E., 2014, MNRAS, 438, 49
Saito S., Takada M., Taruya A., 2008, Phys. Rev. Lett., 100, 191301
Saito S., Takada M., Taruya A., 2009, Phys. Rev. D, 80, 083528
Saito S., Takada M., Taruya A., 2011, Phys. Rev. D, 83, 043529
Samushia L. et al., 2014, MNRAS, 439, 3504
Sánchez A. G. et al., 2012, MNRAS, 425, 415
Sanchez A. G. et al., 2014, MNRAS, 440, 2692
Seljak U., Slosar A., McDonald P., 2006, J. Cosmol. Astropart. Phys., 10, 014
Smee S. et al., 2013, AJ, 146, 32
Smith J. A. et al. [SDSS Collaboration], 2002, AJ, 123, 2121
Smith R. E. et al. [Virgo Consortium Collaboration], 2003, MNRAS, 341, 1311
Spergel D., Flauger R., Hlozek R., 2013, preprint (arXiv:1312.3313)
Takada M., Komatsu E., Futamase T., 2006, Phys. Rev. D, 73 083520
Taruya A., Bernardeau F., Nishimichi T., Codis S., 2012, Phys. Rev. D, 86, 103528
Tereno I., Schimd C., Uzan J.-P., Kilbinger M., Vincent F. H., Fu L., 2009, A&A, 500, 657
Thomas S. A., Abdalla F. B., Lahav O., 2010, Phys. Rev. Lett., 105, 031301
Tojeiro R. et al., 2014, MNRAS, 440, 2222
Verde L., Protopapas P., Jimenez R., 2013, Phys. Dark Universe, 2, 166
Vessot R. F. C. et al., 1980, Phys. Rev. Lett., 45, 2081
Viel M., Haehnelt M. G., Springel V., 2010, J. Cosmol. Astropart. Phys., 06, 015
Villaescusa-Navarro F., Marulli F., Viel M., Branchini E., Castorina E., Sefusatti E., Saito S., 2014, J. Cosmol. Astropart. Phys., 03, 011
von der Linden A. et al., 2014, MNRAS, 443, 1973
Weinheimer C., Degen B., Bleile A., Bonn J., Bornschein L., Kazachenko O., Kovalik A., Otten E. W., 1999, Phys. Lett. B, 460, 219
[KATRIN Collaboration]Wolf J., 2010, Nucl. Instrum. Methods Phys. Res. A, 623, 442
Wong Y. Y. Y., 2008, J. Cosmol. Astropart. Phys., 10, 035
Wyman M., Rudd D. H., Vanderveld R. A., Hu W., 2014, Phys. Rev. Lett., 112, 051302
Xia J.-Q. et al., 2012, J. Cosmol. Astropart. Phys., 06, 010
Zhao G.-B. et al., 2013, MNRAS, 436, 2038
Zheng W., Li H., Xia J.-Q., Wan Y.-P., Li S.-Y., Li M., 2014, Int. J. Modern Phys. D, 23, 1450051

[1]*Lawrence Berkeley National Lab, 1 Cyclotron Rd, Berkeley, CA 94720, USA*
[2]*Kavli Institute for the Physics and Mathematics of the Universe (WPI), Todai Institutes for Advanced Study, The University of Tokyo, Chiba 277-8582, Japan*
[3]*Department of Physics and Astronomy, University of Utah, 115 S 1400 E, Salt Lake City, UT 84112, USA*
[4]*Instituto de Fisica Teorica (UAM/CSIC), Universidad Autonoma de Madrid, Cantoblanco, E-28049 Madrid, Spain*
[5]*Institut de Ciencies del Cosmos, Universitat de Barcelona, IEEC-UB, Martí i Franques 1, E-08028 Barcelona, Spain*
[6]*Institute of Cosmology and Gravitation, Dennis Sciama Building, University of Portsmouth, Portsmouth PO1 3FX, UK*
[7]*Department of Physics, Drexel University, 3141 Chestnut Street, Philadelphia, PA 19104, USA*
[8]*Department of Astronomy and Astrophysics, The Pennsylvania State University, University Park, PA 16802, USA*
[9]*Institute for Gravitation and the Cosmos, The Pennsylvania State University, University Park, PA 16802, USA*
[10]*Max-Planck-Institut fur extraterrestrische Physik, Postfach 1312, Giessenbachstr., D-85748 Garching, Germany*
[11]*Center for Cosmology and Astroparticle Physics, Department of Physics, The Ohio State University, Columbus, OH 43210, USA*
[12]*Center for Cosmology and Particle Physics, New York University, New York, NY 10003, USA*
[13]*Max-Planck-Institute for Astrophysics, Karl-Schwarzschild-Str. 1, D-85748 Garching, Germany*

This paper has been typeset from a TEX/LATEX file prepared by the author.